

Cluster Compounds

Synthesis and Thorough Investigation of Discrete Organotin Telluride Clusters

Jens P. Eußner,^[a, b] Ralph O. Kusche,^[a] and Stefanie Dehnen^{*[a, b]}

Abstract: Systematic experimental and theoretical investigations of reactions of R^1SnCl_3 ($R^1 = CMe_2CH_2C(Me)O$) with $(Me_3Si)_2Te$ allowed for the stepwise formation and single-crystalline isolation of the first tin sesquitelluride clusters

with functional organic ligands. Subsequent derivatization of the latter took place under reorganization of the inorganic core, affording clusters with complex hybrid architectures.

Introduction

The chemistry of Group 14 chalcogenides is now being elaborately studied. Alongside the chemistry of silicates, research evolved to element combinations of higher homologous.^[1] In particular, optoelectronic characteristics of these materials were investigated and showed intriguing properties and potential technical applications.^[2] As compared with the chemistry of tin sulfides and tin selenides, the chemistry of tin tellurides maintains a niche existence because they were found to be "significantly air-sensitive" and "are more difficult to prepare and handle".^[3] Binary anions like $[SnTe_4]^{4-}$, $[Sn_2Te_6]^{4-}$ and $[Sn_4Te_{10}]^{4-}$ as well as ternary anions, such as $\{^1_\infty[HgSnTe_4]^{2-}\}$ and $[M_4(\mu_4-Te)(SnTe_4)_4]^{10-}$ ($M = Mn, Zn, Cd, Hg$), are some of the rare known examples.^[4,5]

Organic decoration, however, enhances the stability of the tin chalcogenide scaffolds. Discrete organotin telluride moieties have thus been stabilized through bulky organic substituents,^[6] donating organometallic or organoelement ligands,^[7] or intramolecular heteroatom coordination of organic ligands.^[8] The tridentate N,C,N-chelating ligand 2,6-(Me_2NCH_2)₂C₆H₃ revealed a series of monoorganotin chalcogenide compounds, inter alia, allowing for the stabilization of terminal $Sn^{II}=Te$ bonds.^[9] In contrast with the numerous polynuclear $(RSn)/S$ and $(RSn)/Se$ complexes containing a variety of organic ligands R , no discrete organotin telluride cage compounds are known at present.

Previous publications of our group describe the synthesis of organogermanium and organotin chalcogenide clusters with

the C,O-chelating ligand $R^1 = CMe_2CH_2C(Me)O$.^[10] Treatment of the keto group at R^1 with hydrazines yields the corresponding hydrazones. Along with the change to the C,N-chelating ligands, rearrangements of the Sn/S or Sn/Se cores into new cluster topologies were observed. Recently, we described the optimization of the syntheses by treating R^1SnCl_3 (**A**) with $(Me_3Si)_2E$ ($E = S, Se$), which enables a directed, stepwise formation of discrete organotin sulfide and selenide moieties.^[11]

Herein, we describe the synthesis and characterization of the first discrete organotin telluride cage compounds, which we obtained through stabilization by C,O- and C,N-chelating ligands. In the course of our systematic studies, we investigated condensation reactions between **A** and $(Me_3Si)_2Te$, yielding different condensation products by control of the stoichiometry of the reagents. The consecutive reaction with hydrazines yielded clusters with different topologies, tailored by the choice of the respective hydrazine derivative. The obtained organo-functionalized bimetallic clusters exhibit low band-gap energies as presented as a proof-of-principle by means of UV/Visible spectroscopy experiments and quantum chemical investigations^[12] using density functional theory (DFT) methods, in particular time-dependent (TD-DFT) calculations.

Results and Discussion

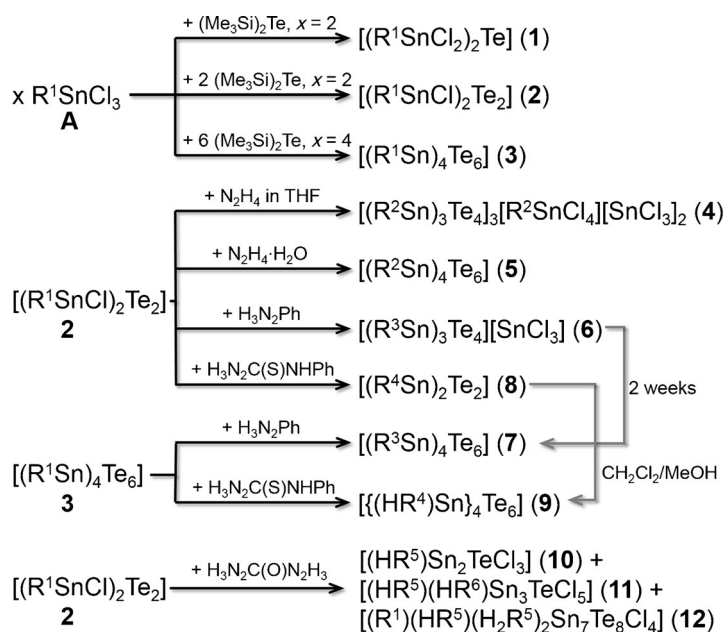
Synthesis

Scheme 1 illustrates the synthesis of the compounds obtained herein. Condensation reactions of R^1SnCl_3 (**A**) and $(Me_3Si)_2Te$ led to the formation of compounds **1–3**. DFT calculations showed that the stepwise condensation is energetically favored, with the generation of Me_3SiCl as the driving force. Derivatization reactions at the organic substituents with different mono-substituted hydrazine derivatives yielded compounds **4–9**. The employment of the bifunctional carbohydrazide $H_3N_2C(O)N_2H_3$ resulted in a complex product mixture. From this, compounds **10–12** were isolated in single crystalline form. All of the reactions were carried out under an inert argon at-

[a] J. P. Eußner, R. O. Kusche, Prof. Dr. S. Dehnen
Fachbereich Chemie, Philipps-Universität Marburg
Hans-Meerwein-Strasse, 35037 Marburg (Germany)
E-mail: dehnen@chemie.uni-marburg.de

[b] J. P. Eußner, Prof. Dr. S. Dehnen
Wissenschaftliches Zentrum für Materialwissenschaften (WZMW)
Philipps-Universität Marburg
Hans-Meerwein-Strasse, 35037 Marburg (Germany)

Supporting information for this article is available on the WWW under <http://dx.doi.org/10.1002/chem.201501666>.



Scheme 1. Synthesis of compounds 1–12. $R^1 = \text{CMe}_2\text{CH}_2\text{C}(\text{Me})\text{O}$; $R^2 = \text{CMe}_2\text{CH}_2\text{C}(\text{Me})\text{NNH}_2$; $R^3 = \text{CMe}_2\text{CH}_2\text{C}(\text{Me})\text{NNHPh}$; $R^4 = \text{CMe}_2\text{CH}_2\text{C}(\text{Me})\text{NNC}(\text{S})\text{NHPH}$; $R^5 = \{\text{CMe}_2\text{CH}_2\text{C}(\text{Me})\text{NN}\}_2\text{C}(\text{O})$; $R^6 = \text{CMe}_2\text{CH}_2\text{C}(\text{Me})\text{NNC}(\text{O})\text{NNH}_2$. The reactions were carried out under inert conditions in CH_2Cl_2 or toluene; for further experimental details see the Supporting Information.

mosphere, under exclusion of light and external moisture. All solvents were dried and freshly distilled prior to use.

The reaction of two equivalents of **A** with one equivalent of $(\text{Me}_3\text{Si})_2\text{Te}$ in toluene, and subsequent layering of the reaction solution with *n*-hexane afforded $[(R^1\text{SnCl}_2)_2\text{Te}]$ (**1**) in 81% yield. Ongoing condensation with another equivalent of $(\text{Me}_3\text{Si})_2\text{Te}$ generated a four-membered Sn_2Te_2 ring in $[(R^1\text{SnCl})_2\text{Te}_2]$ (**2**). This compound formed as an orange precipitate from the toluene solution in 86% yield. Dissolving the precipitate in dichloromethane and layering of the solution with *n*-hexane afforded **2**. At low concentrations, the condensation reaction of **A** with $(\text{Me}_3\text{Si})_2\text{Te}$ in a 1:1.5 stoichiometric ratio in dichloromethane and subsequent layering with *n*-hexane generated $[(R^1\text{Sn})_4\text{Te}_6]$ (**3**) in 52% yield. Higher concentrations of reactants or additional addition of $(\text{Me}_3\text{Si})_2\text{Te}$ led to decomposition and the generation of a brown powder of SnTe .

By using ESI(+) mass spectrometry in dichloromethane solution, we observed a peak with *m/z* corresponding to the $[(R^1\text{Sn})_3\text{Te}_4]^+$ cation.^[13] However, the addition of alkali metal salts of weakly coordinating anions like $[\text{PF}_6]^-$, $[\text{SbF}_6]^-$, or $[\text{BPh}_4]^-$ to stabilize the $[(R^1\text{Sn})_3\text{Te}_4]^+$ cation or careful variations of the stoichiometric ratio of **A** and $(\text{Me}_3\text{Si})_2\text{Te}$ in different solvents failed to promote the crystallization of a $[(R^1\text{Sn})_3\text{Te}_4\text{Cl}]$ (**1**) derivative, which was predicted to be stable according to DFT calculations (see below).

The treatment of **2** in dichloromethane solution with hydrazine (1 mol L⁻¹ in THF) afforded $[(R^2\text{Sn})_3\text{Te}_4]_3[\text{R}^2\text{SnCl}_4][\text{SnCl}_3]_2$ (**4**), whereas the treatment of **2** with hydrazine hydrate yielded $[(R^2\text{Sn})_4\text{Te}_6]$ (**5**). The inorganic core of the $[(R^2\text{Sn})_3\text{Te}_4]^+$ cation in **4** exhibits the defect-heterocubane (DHC) motif. The cationic charge is compensated for by one organotetrachlorido stan-

nate anion $[\text{R}^2\text{SnCl}_4]^-$ and two inorganic $[\text{SnCl}_3]^-$ anions that exhibit Sn atoms in the oxidation state of +II. The $[\text{R}^2\text{SnCl}_4]^-$ anion could be an intermediate prior to the reductive elimination of the organic ligand as one possibility to form the $[\text{SnCl}_3]^-$ anion.^[14] The slightly altered reaction conditions for the generation of **5**, namely, employment of the hydrate instead of a solution of water-free hydrazine in THF, were followed by rapid crystallization within one day; this is in agreement with intense intermolecular interactions within the crystal structure. However, the increased amount of water present under these conditions also accelerates the decomposition of the reaction solutions to form SnTe after several days.

The reaction of phenyl hydrazine with **2** yields the DHC cluster $[(R^3\text{Sn})_3\text{Te}_4][\text{SnCl}_3]$ (**6**, $R^3 = \text{CMe}_2\text{CH}_2\text{C}(\text{Me})\text{NNHPh}$). In a solution of dichloromethane, the condensation reaction proceeds such that the compound $[(R^3\text{Sn})_4\text{Te}_6]$ (**7**) is obtained after two weeks in a sealed NMR test tube as single crystalline material. The generation of larger clusters comes along with an overall energy gain, as shown for the stepwise condensation of the keto-functionalized clusters (see below), which rationalizes the observations. Compound **7** was also obtained directly by the treatment of phenyl hydrazine with **3**.

Thiosemicarbazide $\text{H}_3\text{N}_2\text{C}(\text{S})\text{NHPH}$ reacts with **2** to form $[(R^4\text{Sn})_2\text{Te}_2]$ (**8**, $R^4 = \text{CMe}_2\text{CH}_2\text{C}(\text{Me})\text{NNC}(\text{S})\text{NHPH}$), under retention of the inorganic core, along with two equivalents of HCl and H_2O as side products. The tridentate C,N,S-chelating organic ligand apparently disables the possibility of further condensation for steric reasons. Moreover, we observed the generation of $[(\text{HR}^4)\text{Sn}]_4\text{Te}_6$ (**9**) as another side product when working in a mixture of dichloromethane and methanol. The crystallization of **9** is not observed if working exclusively in dichloromethane solution, whereas **9** crystallizes selectively by treatment of **3** and thiosemicarbazide in a mixture of dichloromethane and methanol with subsequent layering with *n*-hexane.

Employment of the bifunctional carbohydrazide $\text{H}_3\text{N}_2\text{C}(\text{O})\text{N}_2\text{H}_3$ links two tin atoms through multidentate organic HR^5 , H_2R^5 , and HR^6 ($R^5 = \{\text{CMe}_2\text{CH}_2\text{C}(\text{Me})\text{NN}\}_2\text{C}(\text{O})$, $R^6 = \text{CMe}_2\text{CH}_2\text{C}(\text{Me})\text{NNC}(\text{O})\text{NNH}_2$) substituents. The main product of this reaction was **10**, which crystallized after one day. After three days, a smaller quantity of crystals of **11** and **12** formed from the same solution. In **10** and **11**, only one $[\text{Sn}-\text{Te}-\text{Sn}]$ unit is present. Compound **12** consists of an $[\text{Sn}_7\text{Te}_8]$ chain and represents the aggregation product on the route towards a polymeric species, such as ${}^1_{\infty}[\{(\text{C}_2\text{H}_4\text{COO})\text{Sn}\}_2\text{Te}_3]^{2-}$.^[15] Further aggregation seems to be kinetically prohibited by the multidentate organic ligands. The generation of HR^5 and HR^6 ligands took place in situ by deprotonation of the original ligand at the α -position of the central carbonyl unit.

We interpret the observation of compounds **10–12** as an indication for the complex processes and dynamic behavior of organotin tellurides in solution, and as an indication of the rather labile $\text{Sn}-\text{Te}$ bond, which allows for easier fragmentation

in accordance with the DFT results. A similar observation, although with an inverse Ge/E ratio of 1:2 compared with the Sn/Te ratio of 2:1 in **10**, was made with the organogermanium telluride fragment $[R^2GeTe_2]^-$ ($R^2 = CMe_2CH_2C(Me)NNH_2$).^[16] Notably, for E = S or Se, we have not experienced any fragmenta-

tion of the clusters so far, which is in accordance with the greater stability of the according Sn–E bonds.

All of the title compounds were obtained as single crystals (for crystallographic details see Tables 1 and 2) and were further characterized by means of ¹H, ¹³C, ¹¹⁹Sn, and ¹²⁵Te NMR

Table 1. Crystallographic and refinement details of (Me₃Si)₂Te and **1–9** at 100(2) K (Mo_{Kα} radiation, λ = 0.71073 Å, 4·4 CH₂Cl₂ was measured at 250(2) K). For further details, see the Supporting Information.

	(Me ₃ Si) ₂ Te	1	2	3	4·4 CH ₂ Cl ₂
empirical formula	C ₆ H ₁₈ Si ₂ Te	C ₁₂ H ₂₂ Cl ₄ O ₂ Sn ₂ Te	C ₁₂ H ₂₂ Cl ₂ O ₂ Sn ₂ Te ₂	C ₂₄ H ₄₄ O ₄ Sn ₄ Te ₆	C ₆₄ H ₁₁₈ Cl ₁₈ N ₂₀ Sn ₁₂ Te ₁₂
M _r [g mol ⁻¹]	273.98	705.08	761.82	1636.95	4761.61
crystal color and shape	colorless block	yellow needle	orange block	red block	red block
crystal size [mm ³]	0.40 × 0.30 × 0.20	0.45 × 0.13 × 0.12	0.12 × 0.12 × 0.10	0.07 × 0.07 × 0.06	0.23 × 0.18 × 0.18
crystal system	monoclinic	triclinic	monoclinic	monoclinic	monoclinic
space group	C2/c	P $\bar{1}$	P2 ₁ /n	P2 ₁ /n	P2 ₁ /n
a [Å]	9.508(5)	10.1476(7)	8.0853(8)	11.8919(4)	18.0227(5)
b [Å]	11.183(6)	10.6472(6)	12.0453(10)	13.2562(6)	32.9729(12)
c [Å]	11.703(10)	11.1163(7)	11.1735(10)	13.2290(4)	24.5659(7)
α [°]	90	77.251(5)	90	90	90
β [°]	103.94(5)	66.784(5)	104.811(7)	92.284(3)	93.475(2)
γ [°]	90	85.427(5)	90	90	90
V [Å ³]	1207.7(14)	1076.54(12)	1052.03(17)	2083.78(13)	14571.7(8)
Z	4	2	2	2	4
ρ _{calcd} [g cm ⁻³]	1.507	2.175	2.405	2.609	2.170
μ(Mo _{Kα}) [mm ⁻¹]	2.603	4.145	5.344	6.511	4.739
absorption correction type	numerical	numerical	numerical	numerical	numerical
min/max transmission	0.284/0.613	0.207/0.660	0.394/0.405	0.606/0.714	0.386/0.523
2θ range [°]	5.72–53.44	4.36–53.52	4.60–53.54	4.36–53.42	2.72–50.00
measured reflns	4199	4757	5871	29232	74638
R(int)	0.0740	0.0978	0.1529	0.0988	0.0835
independent reflns	1279	3400	2207	4416	25582
independent. reflns [I > 2σ(I)]	1247	3147	2099	3429	10777
parameters/restraints	45/0	196/0	94/0	178/0	1112/205
R ₁ [I > 2σ(I)]/wR ₂ (all data)	0.0350/0.0850	0.0444/0.1185	0.0388/0.0977	0.0411/0.0862	0.0649/0.1785
S (all data)	1.149	1.083	1.147	0.995	0.810
max peak/hole [e ⁻ Å ⁻³]	1.45/–2.13	1.85/–1.57	1.58/–1.86	1.15/–0.86	2.40/–0.89
	5	6·C₆H₁₄	7·3 CH₂Cl₂	8	9·2 MeOH
empirical formula	C ₂₄ H ₅₂ N ₈ Sn ₄ Te ₆	C ₄₂ H ₆₅ Cl ₃ N ₆ Sn ₄ Te ₄	C ₅₁ H ₇₄ Cl ₆ N ₈ Sn ₄ Te ₆	C ₂₆ H ₃₄ N ₆ S ₂ Sn ₂ Te ₂	C ₅₄ H ₈₀ N ₁₂ O ₂ S ₄ Sn ₄ Te ₆
M _r [g mol ⁻¹]	1693.10	1745.33	2252.24	987.29	2297.90
crystal color and shape	red needle	red needle	red block	yellow block	red block
crystal size [mm ³]	0.24 × 0.01 × 0.01	0.50 × 0.04 × 0.03	0.60 × 0.60 × 0.32	0.20 × 0.04 × 0.03	0.08 × 0.08 × 0.03
crystal system	orthorhombic	monoclinic	triclinic	monoclinic	monoclinic
space group	Ccca	P2 ₁ /c	P $\bar{1}$	P2 ₁ /c	P2 ₁ /c
a [Å]	15.5522(5)	11.4360(5)	12.6218(8)	8.0349(3)	11.2842(3)
b [Å]	24.9456(9)	21.7536(7)	12.7680(8)	10.4031(6)	13.4743(3)
c [Å]	22.7771(8)	22.6477(9)	12.9379(8)	20.4275(13)	24.4757(7)
α [°]	90	90	74.290(5)	90	90
β [°]	90	98.917(3)	79.858(5)	101.565(4)	102.777(2)
γ [°]	90	90	61.521(4)	90	90
V [Å ³]	8836.6(5)	5566.1(4)	1761.52(19)	1672.83(16)	3629.30(16)
Z	8	4	1	2	2
ρ _{calcd} [g cm ⁻³]	2.545	2.083	2.123	1.960	2.103
μ(Mo _{Kα}) [mm ⁻¹]	6.144	4.001	4.102	3.353	3.885
absorption correction type	numerical	numerical	numerical	numerical	numerical
min/max transmission	0.521/0.955	0.240/0.889	0.062/0.271	0.603/0.895	0.489/0.890
2θ range [°]	3.36–53.54	2.62–53.52	3.28–53.54	4.08–53.64	3.42–53.48
measured reflns	27617	44985	16048	11108	31932
R(int)	0.1471	0.0798	0.0826	0.0958	0.0471
independent reflns	4702	11783	7443	3537	7688
independent. reflns [I > 2σ(I)]	3199	7236	5856	2628	6808
parameters/restraints	209/4	487/0	364/0	178/0	429/31
R ₁ [I > 2σ(I)]/wR ₂ (all data)	0.0525/0.0779	0.0307/0.0572	0.0541/0.1425	0.0526/0.1443	0.0389/0.0994
S (all data)	0.960	0.832	0.976	1.016	1.069
max peak/hole [e ⁻ Å ⁻³]	1.06/–1.24	0.98/–0.61	2.07/–2.19	1.10/–2.30	1.54/–1.32

Table 2. Crystallographic and refinement details of **10–12** at 100(2) K (Mo_{Kα} radiation, λ = 0.71073 Å). Compound **12·5 CH₂Cl₂** should only be viewed as a structural model. For further details see the Supporting Information.

	10·CH₂Cl₂	11·1.5 CH₂Cl₂	12·5 CH₂Cl₂	12·2 CH₂Cl₂
empirical formula	C ₁₄ H ₂₅ Cl ₅ N ₄ OSn ₂ Te	C _{21.5} H ₃₇ Cl ₈ N ₈ O ₂ Sn ₃ Te	C ₅₀ H ₉₂ Cl ₁₄ N ₁₂ O ₄ Sn ₇ Te ₈	C ₄₇ H ₈₆ Cl ₈ N ₁₂ O ₄ Sn ₇ Te ₈
M _r [g mol ⁻¹]	807.61	1206.86	3273.29	3018.51
crystal color and shape	colorless plates	yellow block	red block	red block
crystal size [mm ³]	0.12 × 0.12 × 0.01	0.21 × 0.15 × 0.10	0.38 × 0.30 × 0.25	0.20 × 0.18 × 0.12
crystal system	monoclinic	monoclinic	triclinic	triclinic
space group	P2 ₁ /c	C2/c	P $\bar{1}$	P $\bar{1}$
a [Å]	7.2831(5)	34.533(2)	18.5622(9)	15.4273(8)
b [Å]	22.8035(14)	11.3986(4)	21.6960(8)	16.5614(8)
c [Å]	15.2834(12)	32.791(2)	26.6656(10)	19.9402(10)
α [°]	90	90	68.646(3)	66.268(4)
β [°]	91.845(6)	139.003(3)	79.599(3)	82.149(4)
γ [°]	90	90	75.079(3)	73.093(4)
V [Å ³]	2537.0(3)	8467.5(8)	9619.4(7)	4461.2(4)
Z	4	8	4	2
ρ _{calcd} [g cm ⁻³]	2.114	1.893	2.260	2.247
μ(Mo _{Kα}) [mm ⁻¹]	3.635	2.967	4.597	4.772
absorption correction type	numerical	numerical	numerical	numerical
min/max transmission	0.669/0.965	0.478/0.690	0.284/0.406	0.471/0.651
2θ range [°]	3.20–50.00	2.60–53.56	2.68–50.00	2.72–53.60
measured reflns	14 287	8946	33 718	40 509
R(int)	0.1211	0.1041	0.1462	0.1137
independent reflns	14 287	8946	33 718	18 876
independent reflns [I > 2σ(I)]	6857	3725	19 533	10 499
parameters/restraints	251/8	403/1	988/8	796/7
R ₁ [I > 2σ(I)]/wR ₂ (all data)	0.0618/0.1437	0.0615/0.1546	0.1756/0.4215	0.0509/0.1224
S (all data)	0.805	0.740	2.269	0.810
max peak/hole [e ⁻ Å ⁻³]	2.14/–1.27	2.06/–1.38	8.44/–3.39	1.95/–1.76

spectroscopy, ESI(+) mass spectrometry, IR and UV/Vis spectroscopy. The qualitative and quantitative elemental composition was verified by EDX spectroscopy. The thermal behavior was investigated by means of simultaneous TGA/DSC experiments. Experimental details are provided in the Supporting Information.

Crystal structures

We report the crystal structure of the widely used volatile reagent (Me₃Si)₂Te (Figure 1, top) for a profound discussion of the obtained compounds. (Me₃Si)₂Te (monoclinic space group C2/c with Z = 4) crystallized by slow cooling from room temperature to 233 K. One-half of the molecule is located in the asymmetric unit with the central Te atom residing on a special position bisected by a C₂ axis. The Si–Te bond length is 2.518(1) Å and the Si–Te–Si angle is 100.92(6)°. The Si–Te bond length is similar to that observed in [(tBuMe₂Si)₂Te], whereas the Si–Te–Si angle is more acute because of the reduced steric influence of the SiMe₃ groups.^[17] There are no Te...Te contacts below 5 Å within the crystal structure.

Compound **1** crystallizes in the triclinic space group P $\bar{1}$ with Z = 2 as yellow needles (Figure 1, center). The molecule consists of two [R¹SnCl₂] fragments that are connected by a μ-Te atom. The Sn–Te bond lengths are 2.7076(5) (Sn1–Te1) and 2.7110(4) Å (Sn2–Te1), and the Sn–Te–Sn angle amounts to 95.05(1)°. The tin atoms possess coordination number of 5 and show trigonal bipyramidal coordination with the two axial positions occupied by O and Cl atoms (O1–Sn1–Cl1: 176.3(1), O2–

Sn2–Cl3: 177.1(1)°). The bidentate organic ligands form intramolecular Lewis acid–base interactions with the central Sn atoms generating a nearly planar, five membered Sn–C–C–C–O ring (C1–Sn1: 2.186(5), C7–Sn2: 2.190(5), O1...Sn1: 2.440(4), O2–Sn2: 2.463(4) Å). Within the Figures 1–8, we depict O→Sn (below N→Sn) coordination as dashed lines to accentuate that the O...Sn distance is considerably larger than the sum of the covalent radii of O and Sn atoms (*r*_{cov}(O–Sn) = 2.03 Å, *r*_{cov}(N–Sn) = 2.11 Å).^[18] The C–Sn–O angles amount to 75.4(2) (Sn1) and 75.1(2)° (Sn2). Sn–Cl bonds to Cl substituents *trans* to O substituents in axial positions (Sn1–Cl1: 2.417(1), Sn2–Cl3: 2.413(1) Å) are slightly longer than the Sn–Cl bonds in the equatorial positions (Sn1–Cl2: 2.384(1), Sn2–Cl4: 2.383(1) Å) because of the intramolecular O→Sn interaction.

Compound **2** crystallizes as orange blocks in the monoclinic space group P2₁/n with Z = 2 (Figure 1, bottom). The molecule possesses crystallographic inversion symmetry, thus including a planar [Sn₂Te₂] four-membered ring (Sn–Te–Sn: 82.43(1), Te–Sn–Te: 97.57(1)°). The Sn1–Te1 bond length is 2.7080(5) Å, thus smaller than that of Sn1–Te1ⁱⁱ (2.7913(5) Å; *ii* = –*x*, 1–*y*, 1–*z*). Again, Sn atoms show trigonal bipyramidal coordination, though having O and Te atoms in the axial positions (O1–Sn1–Te1ⁱⁱ: 176.8(1)°). The replacement of Cl atoms with Te atoms leads to an elongation of the O...Sn distance by about 0.16 to 2.596(6) Å, as a consequence of the strong *trans* effect induced by the Te ligand.

Crystals of **3** form red blocks (space group P2₁/n, Z = 2; Figure 2). The cluster adopts the double-decker-type (DD) topology with two [(R¹Sn)(μ-Te)]₂(μ-Te) units surrounding an in-

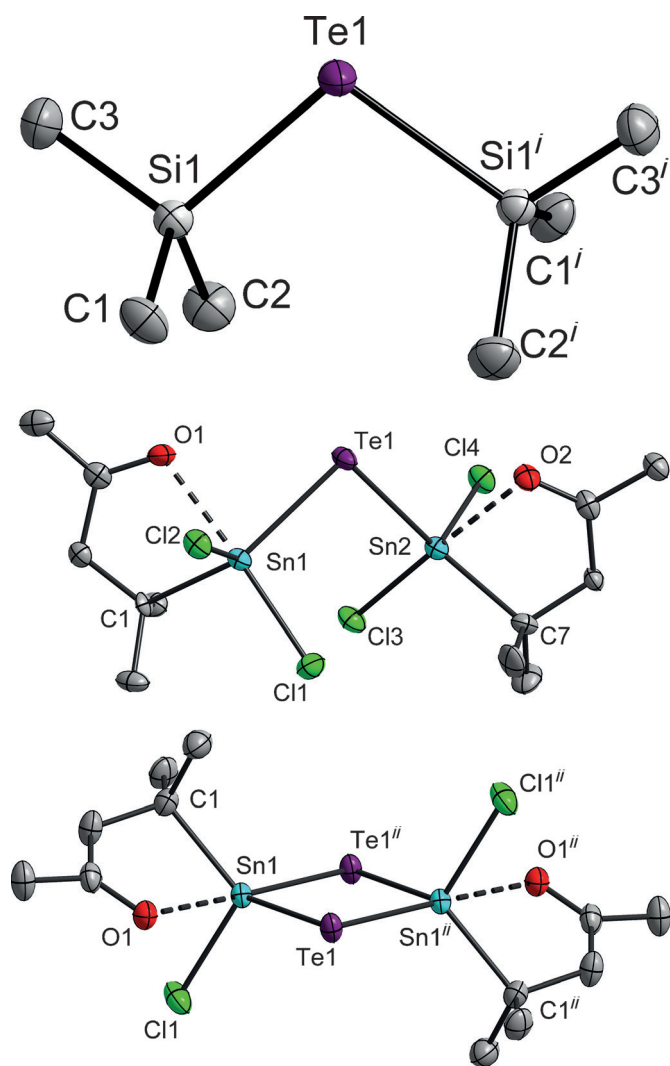


Figure 1. Molecular structures of $(\text{Me}_3\text{Si})_2\text{Te}$ (top), **1** (center), and **2** (bottom) without H atoms. Ellipsoids are drawn at 50%. $i = -x, y, 0.5 - z$; $ii = -x, 1 - y, 1 - z$. Selected structural parameters [\AA , $^\circ$]: $(\text{Me}_3\text{Si})_2\text{Te}$: Si1–Te1 2.518(1), Si1–Te1–Si1' 100.92(6); **1**: Sn1–Te1 2.7076(5), Sn2–Te1 2.7110(4), Sn1–Te1–Te2 95.05(1); **2**: Sn1–Te1 2.7080(5), Sn1–Te1'' 2.7913(5), Sn1–Te1–Sn1'' 82.43(1), Te1–Sn1–Te1'' 97.57(1).

version center. The nearly planar $[\text{Sn}_2\text{Te}_2]$ rings (sum of angles = 359.1°) can be viewed as a fragment of **2**, with similar structural parameters of the inorganic moiety (Sn–Te: 2.7168(7)–2.7915(7) \AA). The Sn1–Te3–Sn2ⁱⁱⁱ angle ($100.11(2)^\circ$; $iii = 1 - x, 1 - y, -z$) is considerably more obtuse than the Sn–Te–Sn angles within the four rings. The organic substituents are pushed out of the plane of four-membered ring, resulting in both an elongation of the C–Sn and Sn...O distances (C1–Sn1: 2.207(7), C7–Sn2: 2.203(7), Sn1...O1: 2.645(5), Sn2...O2: 2.788(6) \AA) and more acute C–Sn–O angles (C1–Sn1–O1: $70.8(2)$, C7–Sn2–O2: $68.5(2)^\circ$). The orientation and sterical demand of the four organic substituents effectively prohibit further aggregation or polymerization. In compounds **1–3** no significant intermolecular contacts are present involving Sn or Te atoms.

According to DFT calculations on such organotin sesquichalcogenide clusters, the DD topology is energetically preferred by 34.1 kJ mol^{-1} over the isomeric hetero-adamantane-type

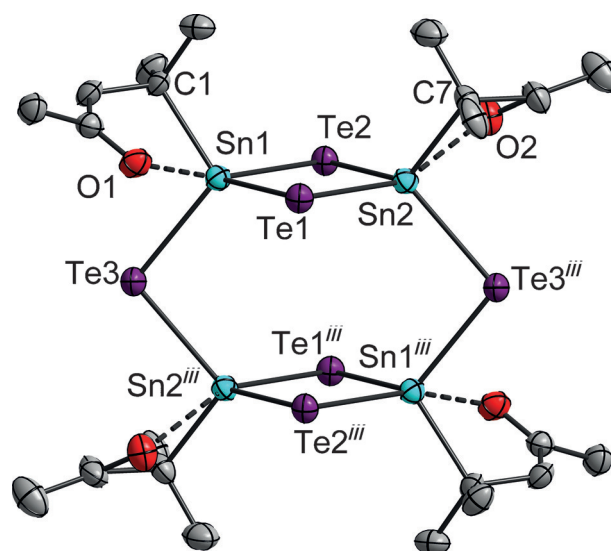


Figure 2. Molecular structure of **3** without H atoms. Ellipsoids are drawn at 50%. $iii = 1 - x, 1 - y, -z$; Selected structural parameters [\AA , $^\circ$]: Sn1–Te1: 2.7324(7), Sn1–Te2: 2.7915(7), Sn1–Te3: 2.7168(7), Sn2–Te1: 2.7778(7), Sn2–Te2: 2.7168(7), Sn2–Te3ⁱⁱⁱ 2.7581(7), Sn1–Te1–Sn2: $84.389(19)$, Sn1–Te2–Sn2: $84.42(2)$, Sn1–Te3–Sn2ⁱⁱⁱ $100.11(2)$, Te1–Sn1–Te2 $95.26(2)$, Te1–Sn1–Te3 $110.51(2)$, Te1–Sn1–Te3 $118.78(2)$, Te1–Sn2–Te2 $95.93(2)$, Te1–Sn2–Te3ⁱⁱⁱ $113.55(2)$, Te2–Sn2–Te3 $118.82(2)$.

(AD) topology because of the realization of a stabilizing intramolecular O→Sn coordination in the first case. The energy difference of the respective isomers increases along the homologous series of $[(\text{R}^1\text{Sn})_4\text{E}_6]$ (E = S, Se, Te) from 14.9 (E = S) through 26.8 (E = Se) to 34.1 kJ mol^{-1} (E = Te); this indicates an even more efficient O→Sn interaction in the DD topology for E = Te as compared with the lighter congeners.

In compounds **1–3**, the Sn–Te bond lengths and Sn–Te–Sn angles are in the range of those observed in known organotin tellurides like $[(\text{R}^7\text{BuSn})_2\text{Te}_2]$,^[9a] $[(\text{R}^7\text{Sn}^{\text{II}})_2\text{Te}]$, $[(\text{R}^7\text{Sn}^{\text{IV}}\text{Te})(\text{R}^7\text{Sn}^{\text{II}})\text{Te}]$ ($\text{R}^7 = 2,6\text{-}(\text{Me}_2\text{NCH}_2)_2\text{C}_6\text{H}_3$),^[9b] $[(\text{R}^8)_2\text{Sn}_3\text{Te}_6]$ ($\text{R}^8 = \text{CH}_2\text{SiMe}_3$),^[19] or the polyanion $^{1-}_\infty\{[(\text{R}^9\text{Sn})_2\text{Te}_3]^{2-}\}$ the polyanion ($\text{R}^9 = \text{C}_2\text{H}_4\text{CO}_2$).^[10] As a result of our systematic studies of organotin chalcogenides with the C,O-bidentate R^1 ligand system, the distinct influence of the different chalcogen atom types (E = S, Se, Te) becomes evident.^[11] The structural consequences are, as expected, elongation of the Sn–E bonds in the order E = S → Se → Te, along with more acute Sn–E–Sn angles.

The condensation reaction of various hydrazines with the keto-groups of the C,O-chelating ligands produce C,N-chelating ligands to coordinate the Sn atoms. This induces a change of the electronic situation at the inorganic core, because of the more effective N→Sn interaction when compared with the O→Sn interaction before. Different topologies and dynamic behavior of organotin chalcogenides in solution, which is well portrayed in the literature.^[20] In general, the isolation of compounds as crystalline material from such dynamic equilibria is based on a lower solubility and favorable intermolecular interactions within the crystal with respect to other species in solution. Accordingly, slight variations of the reaction conditions can provoke the crystallization and isolation of other compounds. The different stability/solubility of a compound with

a certain molecular structure is affected by the steric demand of the substituents, the electronic situation of the substituents, and the tendency of aggregation within solution and/or the crystal.

Compound **4**·4CH₂Cl₂ crystallizes in the monoclinic space group *P2₁/n* with *Z*=4. Compound **4** is a double salt consisting of three [(R²Sn)₃Te₄]⁺ cations besides one [R²SnCl₄]⁻ anion and two [SnCl₃]⁻ anions within the asymmetric unit. The molecular structure of one of the [(R²Sn)₃Te₄]⁺ cations is shown in Figure 3. The inorganic part of the molecule consists of an al-

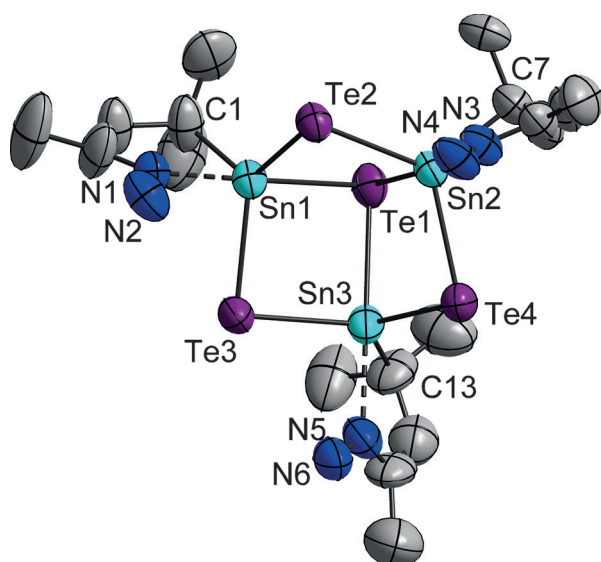


Figure 3. Molecular structure of one of three crystallographically independent [(R²Sn)₃Te₄]⁺ cations in **4**. Ellipsoids are drawn at 30% without H atoms. The larger extension of the thermal ellipsoids are due to the necessity to measure the compound at 250 K to avoid cracking of the crystals (see the Supporting Information). Selected structural parameters [Å, °]: Sn1–Te1 2.902(1), Sn2–Te2 2.757(1), Sn1–Te3 2.748(2), Sn2–Te1 2.929(2), Sn2–Te2 2.757(1), Sn2–Te4 2.757(2), Sn3–Te1 2.953(2), Sn3–Te3 2.750(2), Sn3–Te4 2.741(2). The structural parameters of the inorganic part of the other [(R²Sn)₃Te₄]⁺ cations are similar. Sn–Te 2.742(1)–2.955(2), Sn–Te–Sn 79.87(4)–87.36(4), Te–Sn–Te 92.10(4)–118.30(5).

ternating six-membered Sn–Te ring, which is capped by an additional μ₃-Te atom, thus generating a DHC scaffold. The Sn–Te bond lengths within the six-membered rings are smaller (Sn–μ₃-Te: 2.742(1)–2.765(2) Å) than those involving the μ₃-Te atoms (Sn–μ₃-Te: 2.891(1)–2.955(2) Å); this accords with three N→Sn donating C,N-chelating ligands in the *trans* positions to the μ₃-Te atoms in each cluster (N...Sn: 2.34(1)–2.39(1) Å, N–Sn–μ₃-Te: 173.5(4)–178.5(4)°).

The [(R²Sn)₃Te₄]⁺ cations form intermolecular Te...Te and N–H...Te as well as N–H...N interactions with each other, generating a six-membered cationic chain (see the Supporting Information, Figure S8). Generally, the intermolecular Te...Te distances are longer than the sum of van der Waals radii of two Te atoms (4.16 Å),^[21] except for the considerably smaller Te1...Te5 distance (4.033(1) Å). The anions are situated around the chains and exhibit Sn...Te, Te...Cl, and N–H...Cl interactions, generating a complex three-dimensional network.

The molecular structure of **5** is shown in Figure 4. The compound crystallizes in the orthorhombic space group *Ccca* with *Z*=8. The organotin sesquitelluride cluster is another one to be found in DD topology. The in-plane deformation of the planar [(R²Sn)₂Te₂] ring (sum of angles=360.0°) is more pro-

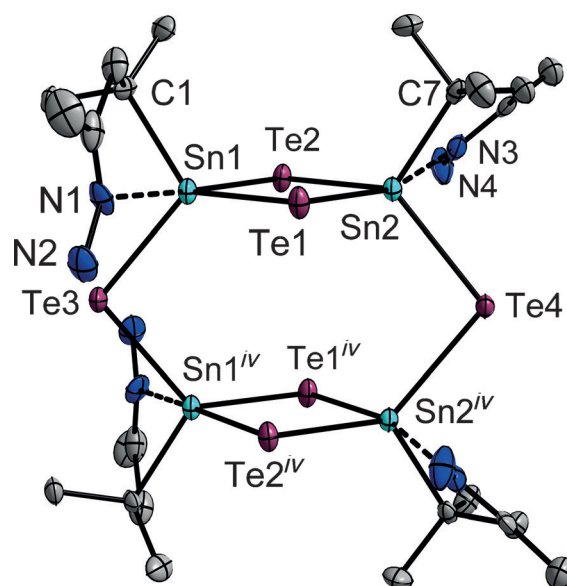


Figure 4. Molecular structure of **5** without H atoms. Ellipsoids are drawn at 50%. *iv* = 0.5–*x*, 1–*y*, *z*; Selected structural parameters [Å, °]: Sn1–Te1: 2.7339(9), Sn1–Te2 2.8349(9), Sn1–Te3 2.7512(8), Sn2–Te1 2.877(1), Sn2–Te2 2.7219(9), Sn2–Te4 2.7700(8), Sn1–Te1–Sn2 85.47(3), Sn1–Te2–Sn1 86.52(3), Sn1–Te3–Sn1^{*iv*} 102.92(4), Sn2–Te4–Sn2^{*iv*} 101.53(4), Te1–Sn1–Te2 94.35(3), Te1–Sn1–Te3 126.11(3), Te2–Sn1–Te3 103.31(3), Te1–Sn2–Te2 93.66(3), Te1–Sn2–Te4 106.60(3), Te2–Sn2–Te4 123.40(3).

nounced here than in the case of the R¹-decorated analogue because of the stronger N→Sn coordination as compared to O→Sn in **3**. The Sn–Te bonds in *trans* position to the N atoms are elongated by about 0.05 to 0.10 Å as compared with the other Sn–Te bonds (in **3** the O→Sn coordination leads to an elongation of 0.02 to 0.06 Å). A C₂ axis runs through Te3 and Te4; this is in agreement with a twist of the inorganic core perpendicular to this axis and a different relative orientation of the organic substituents as compared to **3** (see the Supporting Information, Figure S11). DFT calculations show that the change of conformation has its origin on the molecular level. The observed conformer is more favorable by 9.1 kJ mol⁻¹ as compared to the same complex in the hypothetical, not-observed conformation according to **3**. Contrariwise, the observed molecular conformation of **3** is energetically favored by 7.6 kJ mol⁻¹ over the hypothetical, not-observed conformation according to **5**.

A one-dimensional chain along the crystallographic *a* axis is formed through intermolecular Te...Te and N–H...Te interactions (see the Supporting Information, Figure S12). The intermolecular Te...Te distance (3.521(1) Å) is very short and can be attributed to secondary binding interactions.^[22] Through additional N–H...N hydrogen bonding, a two-dimensional network evolves in the (101) plane.

The reactions of phenyl hydrazine with the keto-functionalized clusters lead to the formation of **6** and **7** (see Figure 5). As compared with the hydrazone groups of **4** and **5**, the phenyl hydrazine group induces a larger steric demand. Again, two different clusters were found, with DHC and DD scaffolds, respectively.

The structural parameters of the inorganic core of the $[(R^3Sn)_3Te_4]^+$ cation within **6** (C_6H_{14} , monoclinic space group $P2_1/c$, $Z=4$) are almost identical to those of the $[(R^2Sn)_3Te_4]^+$ cations in **4**. One $[SnCl_3]^-$ anion per formula unit is present here to compensate for the charge; it closely interacts with the cluster cation by occupying the defect position of the DHC. The resulting heterocubane is naturally distorted in this direction, with additional, relatively short intermolecular Sn...Te contacts (3.7778(6)–3.8106(6) Å). The chlorine atoms of the $[SnCl_3]^-$ counterion are within short intermolecular distances from the

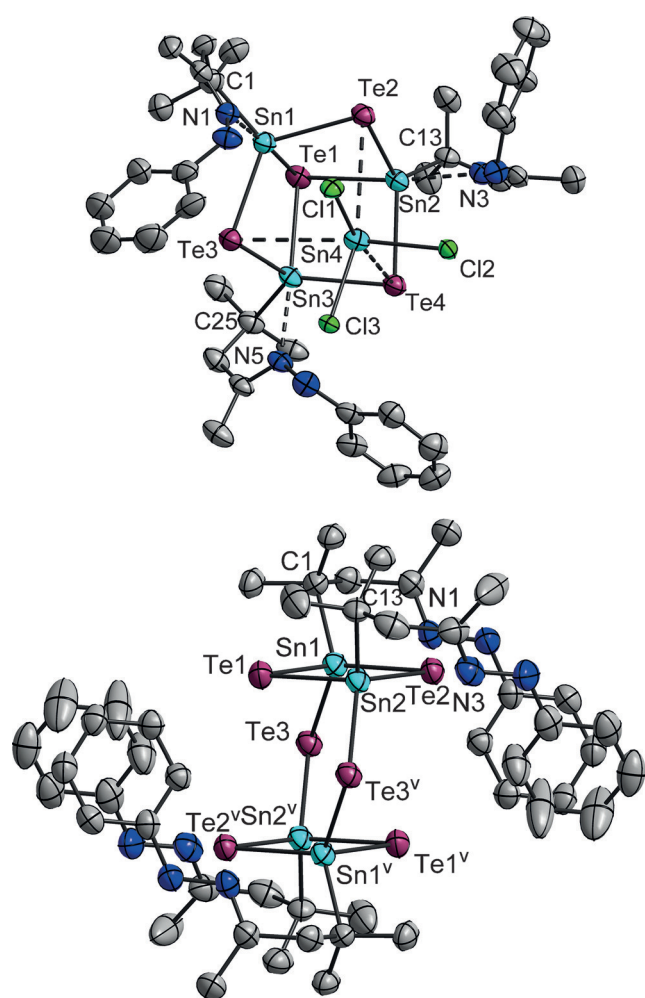


Figure 5. Molecular structure of **6** (top) and **7** (bottom) without H atoms. Ellipsoids are drawn at 50%. $v = 2-x, -y, -z$. Selected structural parameters [$\text{\AA}, ^\circ$]: **6**: Sn1–Te1: 2.9141(6), Sn1–Te2: 2.7668(6), Sn1–Te3: 2.7697(6), Sn2–Te1: 2.9222(6), Sn2–Te2: 2.7627(6), Sn2–Te4: 2.7587(6), Sn3–Te1: 2.9029(6), Sn3–Te3: 2.7580(6), Sn3–Te4: 2.7551(6), Sn–Te–Sn: 79.72(1)–86.70(2), Te–Sn–Te: 92.64(2)–119.28(2); **7**: Sn1–Te1: 2.7461(7), Sn1–Te2: 2.7515(6), Sn1–Te3: 2.7543(6), Sn2–Te1: 2.7567(6), Sn2–Te2: 2.7509(7), Sn2–Te3^v: 2.7524(7), Sn1–Te1–Sn2: 82.50(2), Sn1–Te2–Sn2: 82.50(2), Sn1–Te3–Sn2^v: 100.73(2), Te1–Sn1–Te2: 97.61(2), Te1–Sn1–Te3: 108.64(2), Te2–Sn1–Te3: 121.51(2), Te1–Sn2–Te2: 97.38(2), Te1–Sn2–Te3^v: 106.15(2), Te2–Sn2–Te3^v: 123.10(2).

distal nitrogen atoms of the hydrazone groups of the adjacent cluster (3.303(6)–3.415(5) Å). The combination of short secondary Sn...Te contacts, N–H...Cl hydrogen bonds, and electrostatic interactions might trigger the formation and support the stabilization of this structural motif here. An additional intermolecular and self-complementary Te...Te interaction between adjacent μ_3 -Te atoms (3.9476(8) Å) leads to dimerization (see the Supporting Information, Figure S14).

Although the inorganic core of **7** adopts DD topology ($7 \cdot 3CH_2Cl_2$, triclinic space group $P\bar{1}$, $Z=1$), the molecular structure differs notably from the DD clusters in **3** and **5**. The tin atoms exhibit a coordination number of four and are coordinated in a distorted tetrahedral fashion instead of the trigonal bipyramidal fashion observed in **3** and **5**. The bulky organic substituents apparently prohibit a closer N...Sn approximation (N1...Sn1: 3.126(8) Å, N3...Sn2: 3.130(8) Å).^[23] Hence, the Sn–Te bond lengths are within a very narrow range (Sn–Te: 2.7461(7)–2.7567(6) Å). The organic substituents of each of the $[(R^3Sn)_2Te_2]$ units point into the same direction with regard to the inorganic cluster core, hence providing an optimal steric protection, which results in a kinetically inert cluster.

Notably, the aggregation of Sn/Te clusters has so far stopped at the stage of the organotin sesquitelluride $[Sn_4Te_6]$ core.^[11] In the case of organotin sulfides, further cluster growth to $[(R^3Sn)_4Sn_2S_{10}]$ was observed, which included the generation of two Sn atoms with exclusively inorganic coordination. We have discussed the quoted aggregation as being preferred in the presence of bulky organic ligands.^[12] However, in the case of $E=Te$, the longer Sn–Te bonds obviously comply with a larger steric demand of the organic ligands, such that a rearrangement is not necessary.

Employment of phenyl thiosemicarbazide afforded the complexes $[(R^4Sn)_2Te_2]$ ($R^4 = CMe_2CH_2C(Me)NNC(S)NHPh$; **8**) and $[(HR)^4Sn_4Te_6]$ (**9**), see Figure 6. In **8** (monoclinic space group $P2_1/c$, $Z=2$), the central $[Sn_2Te_2]$ ring connects two C,N,S-tridentate thiosemicarbazide ligands. The π -system of the thiosemicarbazide units is delocalized, which might be represented in the canonical thiol description.

The molecular structure of **8** is analogous to the homologous sulfide compound $[(R^4Sn)_2S_2]$.^[24] Again, the tin atoms exhibit a coordination number of five, in a trigonal bipyramidal fashion with N and Te in axial positions. The stronger *trans* effect of the Te atoms as compared to the S atoms leads to an elongation of the N...Sn distance (N1...Sn1: 2.293(5) Å) compared with that of the homologous complex (2.337(5) Å).

Moreover, we observed the generation of a DD-type cluster in **9** ($9 \cdot 2MeOH$, monoclinic space group $P2_1/c$, $Z=2$). Here, the thiosemicarbazone ligands are observed in the thione form, thus acting as monodentate ligands. Like in **7**, the tin atoms are coordinated in a (distorted) tetrahedral fashion with similar structural parameters of the inorganic core. The nucleophilic character of the thione groups is not sufficiently high to replace the Te atoms within the inorganic core. Instead, they point away from the cluster core and form a two-dimensional hydrogen-bonding network parallel to the (100) plane.

Remarkable results were observed upon treatment of **2** with the bifunctional carbohydrazide $H_3N_2C(O)N_2H_3$, which produced

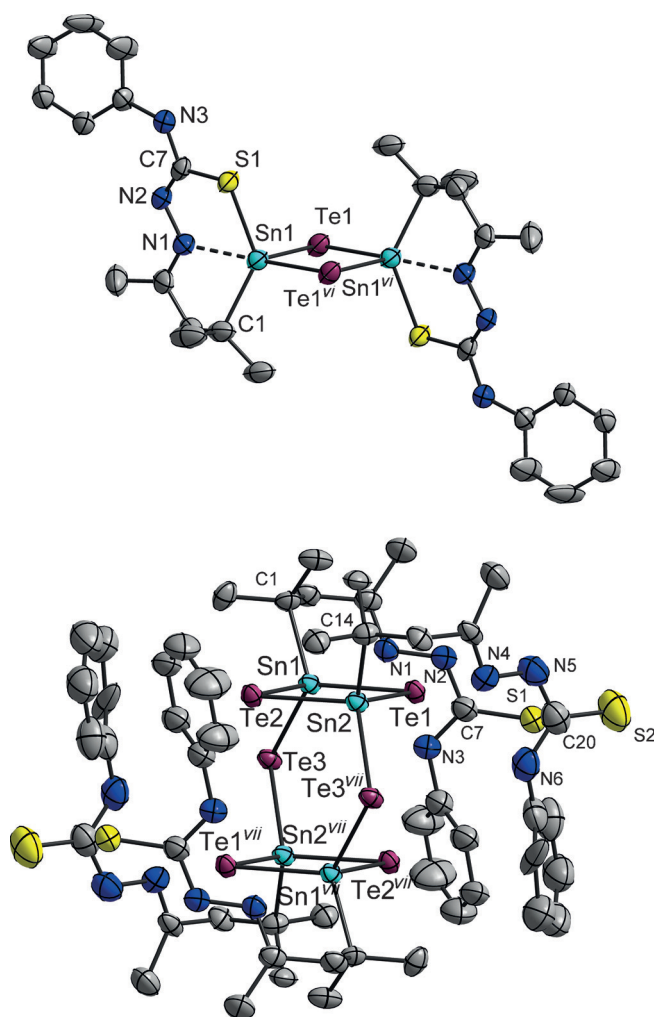


Figure 6. Molecular structures of **8** (top) and **9** (bottom) without H atoms and disorder. Ellipsoids are drawn at 50%. [*vi*] = 1–*x*, –*y*, 1–*z*; [*vii*] = 1–*x*, 1–*y*, 1–*z*. Selected structural parameters [Å, °] for **8**: Sn1–Te1: 2.7256(6), Sn1–Te1^{vi}: 2.8510(7), Sn1–S1: 2.469(1), C7–S1: 1.769(6), Sn1–Te1–Sn1^{vi}: 81.12(2), Te1–Sn1–Te1^{vi}: 98.88(2), S1–Sn1–Te1: 111.75(5), S1–Sn1–Te1^{vi}: 92.98(4); **9**: Sn1–Te1: 2.7446(5), Sn1–Te2: 2.7567(5), Sn1–Te3: 2.7546(5), Sn2–Te1: 2.7391(5), Sn2–Te2: 2.7464(5), Sn2–Te3^{vii}: 2.7629(5), C7–S1: 1.683(7), C20–S2: 1.663(9), Sn1–Te1–Sn2: 81.83(1), Sn1–Te2–Sn2: 81.48(1), Sn1–Te3–Sn2^{vii}: 99.48(2), Te1–Sn1–Te2: 98.15(2), Te1–Sn1–Te3: 121.91(2), Te2–Sn1–Te3: 108.55(2), Te1–Sn2–Te2: 98.53(2), Te1–Sn2–Te3^{vii}: 117.79(2), Te2–Sn2–Te3^{vii}: 110.98(2).

compounds **10**, **11**, and **12**, with so-far unprecedented structural motifs and stronger intramolecular interaction of inorganic and organic moieties. Compound **10** (**10**·CH₂Cl₂, monoclinic space group *P2₁/c*, *Z* = 4) consists of a central [Sn₂TeCl₃] inorganic unit with a pentadentate organic HR⁵ substituent (R⁵ = {CMe₂CH₂C(Me)NN}₂C(O), see Figure 7, top). The Sn–Te bond lengths are slightly longer and the Sn–Te–Sn angle is slightly more acute than in **1**. The pentacoordinate Sn atoms co-exist in trigonal bipyramidal (Sn1) and square pyramidal (Sn2) coordination environment. Both coordination geometries can be continuously transferred into each other by a Berry-type pseudo-rotation, as quantified by the τ parameter ($\tau = 1$ for an ideal trigonal bipyramidal and $\tau = 0$ for an ideal square pyramidal coordination).^[25] For Sn1 τ is 0.82, with Cl1 and N1 in the axial positions, whereas for Sn2 τ is 0.02. The basal positions in

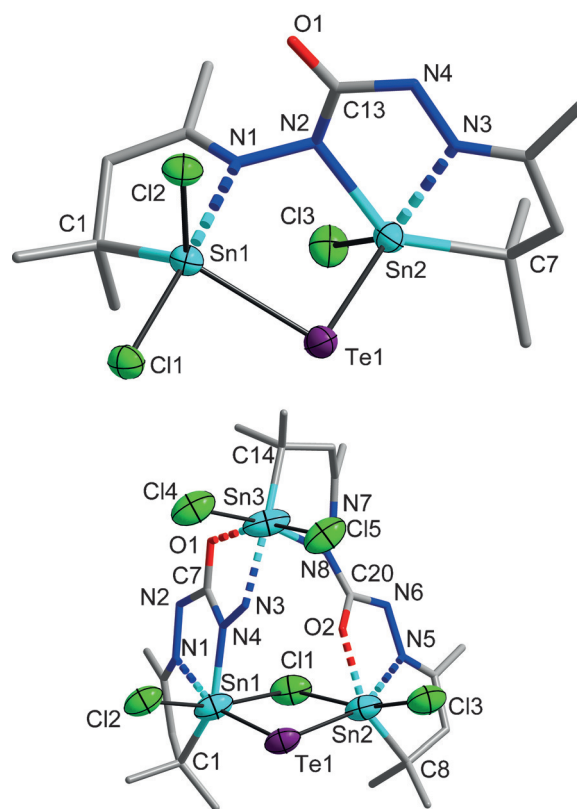


Figure 7. Molecular structures of **10** (top) and **11** (bottom). Ellipsoids are drawn at 50%. Organic substituents are denoted as sticks without H atoms. Selected structural parameters [Å, °]: **10**: Sn1–Te1: 2.7346(12), Sn2–Te1: 2.7290(12), Sn1–Te1–Sn2: 94.11(3); **11**: Sn1–Te1: 2.768(1), Sn2–Te1: 2.750(1), Sn1–Cl1: 2.655(3), Sn2–Cl1: 2.829(3), Sn1–Te1–Sn2: 92.48(3), Sn1–Cl1–Sn2: 93.17(8), Cl1–Sn1–Te1: 87.89(7), Cl1–Sn2–Te1: 84.88(7).

the coordination polyhedron around Sn2 are occupied by C7, N2, N3, and Te1, and the apical position by Cl3. N2 is deprotonated, as rationalized by a short N2–Sn1 bond (2.142(8) Å). The deprotonation of the organic HR⁵ substituent at N2 induces the different coordination at Sn2, as is also shown below for **12**. The carbohydrazide unit activates self-complementary N–H...O hydrogen-bonding interactions through O1 and the N4 (see the Supporting Information, Figure S22).

The central structural motif of the molecular structure of **11** (**11**·1.5CH₂Cl₂, monoclinic space group *C2/c*, *Z* = 8) is an asymmetric Sn–Te–Sn–Cl four-membered ring (see Figure 7, bottom). All the tin atoms exhibit a distorted octahedral coordination, which has been unprecedented in RSn/E cluster chemistry (E = S, Se, Te). The pentadentate HR⁵ and HR⁶ (R⁶ = CMe₂CH₂C(Me)NNC(O)NNH₂) ligands connect the Sn–Te–Sn–Cl four-membered ring with Sn3. The organic ligands are deprotonated at N4 and N8, causing short N–Sn bonds. Notably, the HR⁶ organic ligand does not undergo condensation with the keto group of an R¹ ligand. Instead, the ligand realizes self-complementary N–H...Cl interactions. Within the Sn–Te–Sn–Cl ring the Sn–Te bond lengths differ by only 0.018 Å, whereas the Sn–Cl bond lengths differ much more notably, by 0.174 Å. The Sn–Te–Sn angle (92.48(3)°) is more acute than the Sn–Cl–Sn (93.17(8)°) angle.^[26]

Compound **12** was obtained in two pseudo-polymorphic crystalline modifications. Complex **12**·5CH₂Cl₂ (triclinic space group $P\bar{1}$, $Z=4$) crystallizes directly from a dichloromethane solution upon layering with *n*-hexane. Because of rapid decomposition of the crystals, we only present a structural model of the compound and do not discuss structural details. Complex **12**·2CH₂Cl₂ (triclinic space group $P\bar{1}$, $Z=2$) formed through a crystal-to-crystal transformation from **12**·5CH₂Cl₂ upon loss of three molecules of dichloromethane per cluster molecule in the inert oil used for the crystallographic investigation within one day. We observed cracks within the transformed crystal under a light-microscope; however, the crystals of the second pseudo-polymorph produce a homogeneous diffraction pattern. During the transformation, the cell volume per formula unit decreases by about 348 Å³, which confirms to the loss of three solvent molecules of dichloromethane. Suspending **12**·2CH₂Cl₂ in dichloromethane led to decomposition of the crystals, hence we were not able to check the reversibility of the transformation.

In the relatively complicated cluster architecture in **12** (see Figure 8), a [Sn₇Te₈Cl₄] backbone is linked by two H₂R⁵ ligands and one HR⁵ ligand. The H₂R⁵ ligands connect Sn1 with Sn5 and Sn2 with Sn4. The HR⁵ ligand connects Sn6 with Sn7 (N7–Sn7: 2.158(10) Å). Sn3 remains isolated and exhibits an R¹ ligand. Intramolecular N–H...O hydrogen-bonding interactions generate a molecular capsule. The inorganic backbone comprises a sequence of an [Sn₂Te] moiety, two [Sn₂Te₂] rings and one Sn atom, which are connected by three μ-Te atoms. Additional chlorine substituents are coordinated to Sn1, Sn2, and Sn7. The tin atoms show different coordination numbers and coordination environments. Sn4 and Sn5 exhibit a tetrahedral environment. Sn1 ($\tau=0.34$), Sn2 ($\tau=0.44$), Sn3 ($\tau=0.96$), Sn6 ($\tau=0.84$) are coordinated in a distorted trigonal bipyramidal fashion. Again, the deprotonation of the organic HR⁵ ligand provokes a quadratic pyramidal coordination environment at

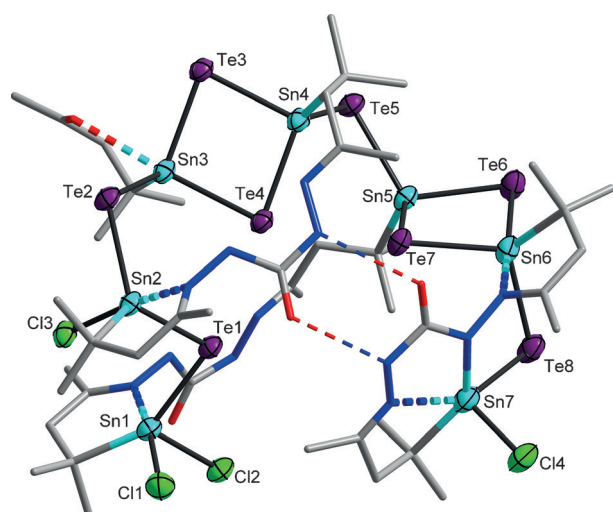


Figure 8. Molecular structure of **12** in **12**·2CH₂Cl₂. Ellipsoids are drawn at 50%. Organic substituents are denoted as sticks without H atoms. Selected structural parameters [Å, °]: Sn–Te: 2.732(1)–2.882(1), Sn–Te–Sn: 81.19(3)–100.38(3), Te–Sn–Te: 94.94(3)–121.57(3).

Sn7 ($\tau=0.16$). At the inner side of the inorganic scaffold short intermolecular Te...Te distances are observed (Te1...Te4: 3.500(1) Å, Te4...Te7: 3.542(1) Å). Intermolecular hydrogen bonding leads to a dimerization through N–H...O self-complementary interactions.

NMR Spectroscopy

¹¹⁹Sn and ¹²⁵Te NMR experiments in CD₂Cl₂ and CDCl₃ give insights to the integrity and potential dynamic behavior of the clusters in solution. The signals are sharp for small complexes **1** and **2**. The reduced solubility of the larger complexes as well as dynamic processes in solution leads to broadening of the signals under loss of the fine structure. For these reasons, ²J(¹¹⁷Sn–¹¹⁹Sn) and ¹J(¹¹⁹Sn–¹²⁵Te) coupling constants were only determined for **1** and **2** (¹J(¹¹⁷Sn–¹²⁵Te) satellites were also observed, but are not given here). ¹H and ¹³C NMR spectra of the compounds show the expected resonances of the organic ligands.

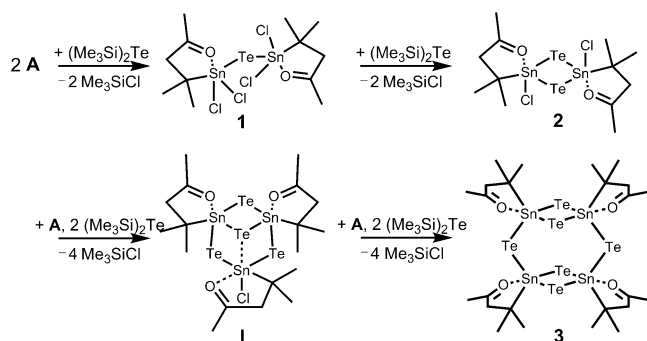
The successive generation of Sn–Te bonds leads to a significant shift to higher fields in the ¹¹⁹Sn NMR spectroscopic experiments (**1**: $\delta=-272$, **2**: $\delta=-546$, **3**: $\delta=-577$ ppm). The variations in the coupling constants ²J(¹¹⁷Sn–¹¹⁹Sn) (**1**: 387, **2**: 156 Hz) and ¹J(¹¹⁹Sn–¹²⁵Te) (**1**: 4.72, **2**: 2.64 kHz) reflect the different molecular geometry of each complex and are in agreement with known organotin complexes with this structural motif.^[27] Contrariwise to the ¹¹⁹Sn NMR data, the ¹²⁵Te NMR signals are shifted to the lower field (**1**: $\delta=-287$, **2**: $\delta=212$ ppm).

The hydrazone complexes show further shift to higher field in the ¹¹⁹Sn NMR spectra (**5**: $\delta=-680$ ppm). Within the ¹²⁵Te NMR spectra, the Te atoms within the alternating four-membered ring in **5** accord with a signal at $\delta=483$ ppm, whereas the Te atoms between the rings produce a signal at $\delta=-660$ ppm. In **6**, the two signals at $\delta=-844$ and $\delta=449$ ppm can be assigned to the μ-Te atoms and the μ₃-Te atom, respectively, according to the expected significant upfield shift with increasing coordination number.

Two signal sets are found in the NMR spectra of **8** with an intensity of approximately 1:1. In the ¹¹⁹Sn NMR spectrum, two narrow signals are found at $\delta=-601$ and -605 ppm. These signals most probably arise from an equilibrium of two isomers in solution with the crystallographically determined *trans* arrangement and a (hypothetic) *cis* arrangement of the organic substituents (see the Supporting Information, Figure S32), respectively. DFT calculations confirm a shift of 4 ppm to higher field in the ¹¹⁹Sn NMR spectrum, and a slightly higher energy of the *cis* isomer is observed (+5.2 kJ mol⁻¹; for further details see the Supporting Information).

DFT Calculations

The consecutively performed, stepwise reactions of **A** with (Me₃Si)₂Te was additionally studied by means of quantum chemical investigations employing density functional theory (DFT) methods. The condensation cascade that was subject to the studies is outlined in Scheme 2.



Scheme 2. Proposed reaction for the stepwise formation of the organotin telluride cage compound **3** and basic concept of the quantum chemical analysis.

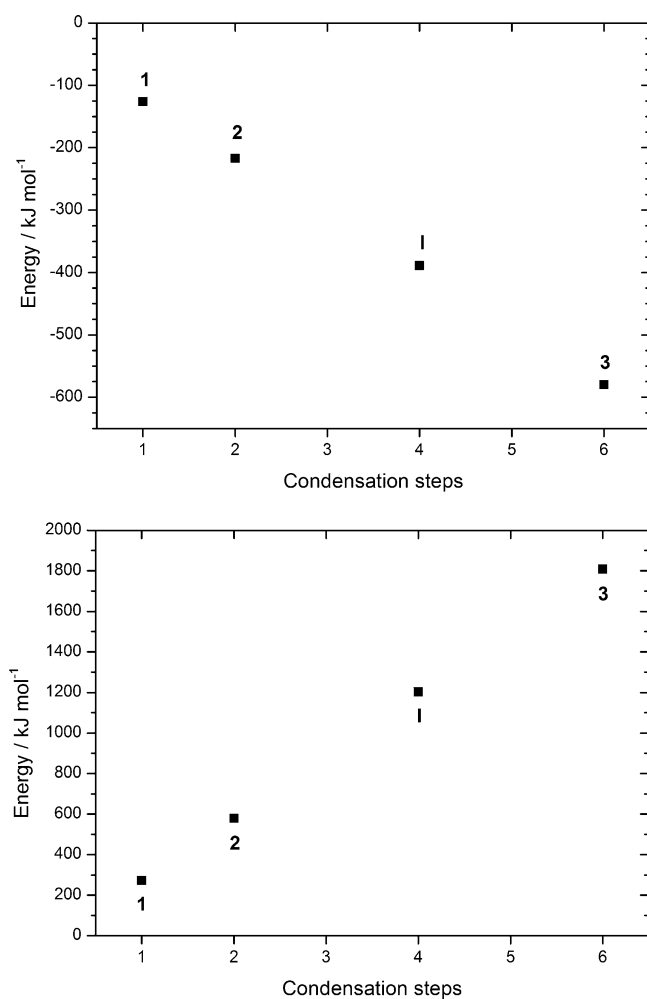


Figure 9. DFT analysis of the formation pathway. Relative energies for the formation of molecules **1**, **2**, **I**, and **3** are given in kJ mol^{-1} . Top: Total reaction energies, as calculated by subtraction of the sum of the total energies of the starting materials **A** and $(\text{Me}_3\text{Si})_2\text{Te}$ from the sum of the total energies of the respective species plus Me_3SiCl as side product. The total energy decreases by about 47 kJ mol^{-1} per newly created Sn–Te bond. Bottom: Reaction energies disregarding the energy differences within the silyl reactants, namely the energy differences between (formed) Si–Cl and (broken) Si–Te bonds in Me_3SiCl and $(\text{Me}_3\text{Si})_2\text{Te}$, respectively, which amounts to approximately 199 kJ mol^{-1} per newly created Sn–Te bond. Details are provided in the Supporting Information.

The common driving force for all of the condensation steps is the generation of the extraordinary stable Si–Cl bond in Me_3SiCl , with an energy of about 468 kJ mol^{-1} , under cleavage of the weak Si–Te bond in $(\text{Me}_3\text{Si})_2\text{Te}$, with an energy of about 269 kJ mol^{-1} [28].

The overall energy decreases by about 94 kJ mol^{-1} per condensation step (see Figure 9, top). This suggests that all of the presented species should be predominant at a certain stage of the condensation cascade. As pointed out above, we were not able to isolate species **I**. Figure 9 (bottom) illustrates the increasingly labile character of the obtained clusters. Whereas the overall energy for the generation is negative, replacement of Sn–Cl bonds for Sn–Te bonds results in the shown course of the cluster stabilities.

Calculations of the natural charges through natural population analysis (NPA) [29] of the DFT wave function give small positive values of about $+0.9$ to $+1.1$ at the formal Sn^{IV} atoms in the organotin sesquitelluride clusters (see the Supporting Information, Table S16), beside small negative values of -0.4 to -0.5 at the Te atoms. The small charges accord with nearly identical electronegativities of Sn and Te. Low polarity of the inorganic cluster core in combination with the high steric demand of the organic ligand obviously enabled the isolation of discrete organotin telluride compounds.

Time-dependent DFT calculations (TD-DFT) of the singlet and triplet excitation energies of **1**, **2**, **I**, and **3** underline the observed bathochromic shift upon expansion of the inorganic core. [30] The minimum singlet excitation energy drops significantly from about 3.0 in **1** to 2.2 eV in **3** (see Figure 10). This can be attributed to the increasing energy level of the highest occupied molecular orbital (HOMO; with highest contribution of Te 5p atomic orbitals (AOs)), which is excited into energetically low-lying antibonding orbitals involving RSn units that do not differ as notably in energy as the HOMO level for the different (RSn)/E systems. The relatively low absorption energy, situated within the visible-light range, is also in perfect agreement with the observed light sensitivity of the compounds in solution.

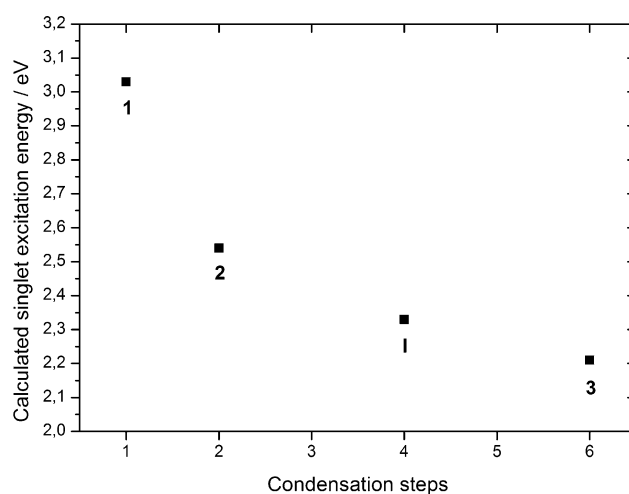


Figure 10. Singlet excitation energies with increasing cluster core size, as calculated by means of time-dependent DFT calculations.

Conclusion

We have shown that discrete organotin telluride clusters can be stabilized, and thus be isolated, by attachment of C,O- and C,N-chelating ligands. These clusters can be obtained by stepwise condensation reactions of the organotin trichloride R^1SnCl_3 and $(Me_3Si)_2Te$ to yield $[(R^1SnCl_2)_2Te]$ (**1**), $[(R^1SnCl)_2Te_2]$ (**2**), and $[(R^1Sn)_4Te_6]$ (**3**). The treatment of **2** and **3** with different substituted hydrazines yielded a large variety of corresponding hydrazine derivatives, with or without rearrangement of the inorganic cluster core (**4–12**).

We further envisage exploring the photophysical properties and thermochemical processes of organotin telluride compounds as materials with fine-tuneable physical and chemical properties.

Experimental Section

General

All manipulations were performed under argon atmosphere and strict exclusion of light. All solvents were dried and freshly distilled prior to use. R^1SnCl_3 ^[31] was prepared according to reported methods, $(Me_3Si)_2Te$ was prepared as described below. Other reagents were purchased from Sigma–Aldrich. 1H -, ^{13}C -, ^{31}Si -, ^{119}Sn -, and ^{125}Te NMR spectroscopic measurements were carried out using a Bruker DRX 250 MHz, DRX 300 MHz, DRX 400 MHz, and DRX 500 MHz spectrometer at 25 °C. The chemical shifts were quoted in ppm relative to the residual protons of deuterated solvents in the 1H NMR and ^{13}C NMR spectra. Me_4Si , Me_4Sn , and Me_2Te were used as external standard for ^{29}Si , ^{119}Sn , and ^{125}Te NMR measurements. MS (ESI) measurements were performed on a Thermo Fischer Scientifics Finnigan LTQ-FT. IR spectroscopy was performed with a Bruker Tensor 37 between 4000 and 400 cm^{-1} ($\pm 0.01 cm^{-1}$) in attenuated total reflection. Elemental analysis was performed on an Elementar vario micro apparatus. Energy-dispersive X-ray spectroscopy analysis, EDX, was performed using the EDX device Voyager 4.0 of Noran Instruments coupled with the electron microscope CamScan CS 4DV. Data acquisition was performed with an acceleration voltage of 20 kV and 100 s accumulation time. UV/Vis spectra were measured on a Varian Cary 5000 spectrometer in reflectance. Thermogravimetric analysis (TGA) and differential scanning calorimetry (DSC) were performed simultaneously on a Netzsch STA 400 in an aluminium oxide crucible in argon atmosphere with a heating rate of 10 $Kmin^{-1}$.

Syntheses

(Me_3Si) $_2Te$: Prepared by varying the reported method for the synthesis of $(Me_3Si)_2Se$ reported by Schmidt and Ruf.^[32] Ammonia (250 mL) was condensed onto sodium (5.90 g, 257 mmol) at -40 °C. Tellurium (16.5 g, 130 mmol) was added slowly in small portions. The mixture was stirred for 4 h at -40 °C and slowly warmed up to room temperature thereupon. Ammonia was allowed to evaporate, and the resulting colorless powder (Na_2Te) was dried in vacuum. It was subsequently suspended in THF (250 mL) and freshly distilled Me_3SiCl (32 mL, 252 mmol) was added. The solution was heated at reflux for 3 h and filtered. THF was removed in vacuo. The product was obtained as colorless liquid by fractional distillation under reduced pressure. Yield: 22.8 g (83.2 mmol, 65%). 1H NMR (400 MHz, $CDCl_3$): $\delta = 0.50$ ppm (s, $^1J(^1H-^{13}C) = 121.0$ Hz, 18H); ^{13}C NMR (101 MHz, $CDCl_3$): $\delta =$

5.53 ppm (s, $^1J(^{13}C-^{29}Si) = 50.4$ Hz, $^2J(^{13}C-^{125}Te) = 6.9$ Hz); ^{29}Si NMR (79 MHz, $CDCl_3$): $\delta = -4.94$ ppm (s, $^1J(^{29}Si-^{125}Te) = 275$ Hz, $^1J(^{29}Si-^{13}C) = 50.4$ Hz); ^{125}Te NMR (126 MHz, $CDCl_3$): $\delta = -853$ ppm (s, $^1J(^{125}Te-^{29}Si) = 275$ Hz).

Compound 1: R^1SnCl_3 (0.500 g, 1.54 mmol) was dissolved in toluene (10 mL). $(Me_3Si)_2Te$ (0.106 g, 0.385 mmol) was added at room temperature. It was then stirred for 24 h. The solution was layered with *n*-pentane (10 mL). Yellow crystals of compound **1** formed within one day, which were collected and dried in high vacuum. Yield: 0.22 g (0.31 mmol, 81% calculated on the basis of $(Me_3Si)_2Te$). M.p.: 145 °C (decomposition). 1H NMR (300 MHz, $CDCl_3$): $\delta = 1.40$ (s, $^3J(^1H-^{119}Sn) = 179$ Hz, 12H, Me_2), 2.40 (s, 6H, Me), 2.98 ppm (s, $^3J(^1H-^{119}Sn) = 183$ Hz, 4H, CH_2); ^{13}C NMR (75 MHz, $CDCl_3$): $\delta = 25.05$ (Me_2), 29.17 (Me), 44.73 (CSn), 54.72 (CH_2), 214.41 ppm (CO); ^{119}Sn NMR (149 MHz, $CDCl_3$): $\delta = -272$ ppm (s, $^1J(^{119}Sn-^{125}Te) = 4.72$ kHz, $^2J(^{119}Sn-^{117}Sn) = 387$ Hz); ^{125}Te NMR (126 MHz, $CDCl_3$): $\delta = -287$ ppm (s, $^1J(^{125}Te-^{119}Sn) = 4.72$ kHz); IR: $\tilde{\nu} = 3344.2$ (w), 3251.2 (w), 3143.3 (w), 2951.7 (m), 2854.1 (m), 2830.1 (m), 1660.7 (s), 1499.7 (w), 1459.3 (m), 1389.8 (w), 1368.8 (m), 1332.4 (m), 1259.1 (w), 1239.4 (w), 1187.2 (m), 1139.3 (w), 1116.5 (m), 1021.5 (w), 965.6 (w), 801.3 (w), 624.5 (s), 499.3 cm^{-1} (m); UV/Vis (onset): 2.6 eV; EDX: calcd Sn/Te/Cl = 2.00:1.00:4.00; found: Sn/Te/Cl = 2.00:1.00:3.98.

Compound 2: R^1SnCl_3 (0.500 g, 1.54 mmol) was dissolved in toluene (10 mL). $(Me_3Si)_2Te$ (0.423 g, 1.54 mmol) was added at 0 °C. It was stirred for 30 min and warmed up to room temperature. The resulting yellow precipitate was filtered and washed with toluene. Orange crystals of compound **2** formed within one day upon dissolving the yellow precipitate in dichloromethane and layering with *n*-pentane. Yield: 0.51 g (0.67 mmol, 86% calculated on the basis of $(Me_3Si)_2Te$). M.p.: 134 °C (decomposition); 1H NMR (300 MHz, $CDCl_3$): $\delta = 1.12$ (s, $^3J(^1H-^{119}Sn) = 160$ Hz, 12H, Me_2), 2.28 (s, 6H, Me), 2.59 (s, $^3J(^1H-^{119}Sn) = 148$ Hz, 4H, CH_2) ppm; ^{13}C NMR (75 MHz, $CDCl_3$): $\delta = 25.68$ (Me_2), 30.19 (Me), 46.78 (CSn), 54.55 (CH_2), 204.54 ppm (CO); ^{119}Sn NMR (149 MHz, $CDCl_3$): $\delta = -546$ ppm (s, $^1J(^{119}Sn-^{125}Te) = 2.64$ kHz, $^2J(^{119}Sn-^{117}Sn) = 165$ Hz); ^{125}Te NMR (126 MHz, $CDCl_3$): $\delta = 212$ ppm (s, $^1J(^{125}Te-^{119}Sn) = 2.64$ kHz); IR: $\tilde{\nu} = 3135.0$ (w), 3047.0 (w), 2927.3 (w), 2842.4 (m), 1687.7 (s), 1452.6 (w), 1408.0 (w), 1378.1 (w), 1358.5 (m), 1332.7 (w), 1234.9 (w), 1174.2 (s), 1111.6 (m), 1014.9 (w), 956.7 (w), 837.1 (w), 606.7 cm^{-1} (m); UV/Vis (onset): 2.1 eV; EDX: calcd Sn/Te/Cl = 1.00:1.00:1.00; found: Sn/Te/Cl = 1.00:0.99:0.92; elemental analysis calcd (%) for $C_{12}H_{22}Cl_2O_2Sn_2Te_2$: C 18.92, H 2.91; found: C 18.71, H 2.79.

Compound 3: R^1SnCl_3 (0.100 g, 0.308 mmol) was dissolved in dichloromethane (10 mL). $(Me_3Si)_2Te$ (0.126 g, 0.462 mmol) was added at room temperature. The solution was stirred for 5 h. The intensive red solution was layered with *n*-pentane (10 mL). Red crystals of compound **3** formed within one day, which were collected and dried in high vacuum. Yield: 0.065 g (0.040 mmol, 52% calcd on the basis of $(Me_3Si)_2Te$). M.p.: 146 °C (decomposition); 1H NMR (300 MHz, CD_2Cl_2): $\delta = 1.14$ (s, $^3J(^1H-^{119}Sn) = 136$ Hz, 24H, Me_2), 2.21 (s, 12H, Me), 2.54 ppm (s, $^3J(^1H-^{119}Sn) = 124$ Hz, 8H, CH_2); ^{13}C NMR (75 MHz, CD_2Cl_2): $\delta = 26.38$ (Me_2), 27.91 (Me), 30.50 (CSn), 55.55 (CH_2), 211.04 ppm (CO); ^{119}Sn -NMR (112 MHz, CD_2Cl_2): $\delta = -577$ ppm; ^{125}Te NMR (126 MHz, CD_2Cl_2): no signal found; IR: $\tilde{\nu} = 2840.7$ (w), 1690.6 (s), 1451.0 (w), 1391.9 (w), 1354.6 (w), 1326.9 (m), 1323.9 (m), 1173.9 (s), 1110.2 (s), 1012.0 (w), 958.6 (w), 835.8 (m), 716.7 (m), 607.5 cm^{-1} (s); UV/Vis (onset): 1.9 eV; HRMS (ESI): m/z calcd for $[C_{18}H_{33}O_3Sn_3Te_4]^+$ ($[M-C_6H_{11}OSnTe_4]^+$): $m/z = 1164.5688$; found: 1164.5714; EDX: calcd Sn/Te = 0.67:1.00; found: Sn/Te = 0.69:1.00.

Compound 4: Compound **2** (0.050 mg, 0.066 mmol) was dissolved in dichloromethane (10 mL). A hydrazine solution (0.35 mL,

1 mol L⁻¹ in THF) was added at room temperature. The resulting orange solution was stirred for 30 min and subsequently layered with *n*-hexane (10 mL). Red crystals of compound **4**·4CH₂Cl₂ formed within one day, which were collected and dried in high vacuum. They were insoluble in all common organic solvents. Yield: 0.010 g (2.3 μmol, 21% calculated on the basis of **2**). IR: $\tilde{\nu}$ = 3648.6 (w), 3334.0 (w), 3208.6 (w), 2980.5 (m), 2844.6 (m), 2286.6 (w, br), 2148.6 (w), 2049.9 (w), 1980.3 (w), 1660.3 (m), 1608.5 (m), 1584.8 (m), 1426.4 (m), 1382.1 (m), 1249.2 (m), 1203.8 (m), 1143.6 (s), 1095.3 (s), 1003.4 (m), 956.2 (m), 845.0 (s), 800.5 (s), 732.0 (s), 657.8 (s), 585.8 (w), 510.8 (w), 493.2 (w), 469.4 (w), 434.5 cm⁻¹ (w); HRMS (ESI): *m/z* calcd for [C₁₈H₃₉N₆Sn₃Te₄]⁺: 1206.6494; found: 1206.6515; EDX: calcd Sn/Te = 1.00:1.00; found: Sn/Te = 1.00:1.04 (Cl was not considered because of dichloromethane solvent molecules).

Compound 5: Compound **2** (0.10 g, 0.13 mmol) was dissolved in dichloromethane (10 mL). N₂H₄·H₂O (0.03 mL, 50–60% N₂H₄) was added at room temperature. A red cloudy precipitate appeared rapidly within the solution, but re-dissolved after 15 min. After 30 min, the deep-red solution was layered with *n*-hexane (10 mL). Red crystals of compound **5** formed within one day, which were collected and dried in high vacuum. Yield: 40 mg (0.024 mmol, 55% calculated on the basis of **2**). M.p.: 150 °C (decomposition); ¹H NMR (300 MHz, CDCl₃): δ = 1.08 (s, ³J(¹H-¹¹⁹Sn) = 135 Hz, 24H, Me₂), 1.84 (s, 12H, Me), 2.32 (s, ³J(¹H-¹¹⁹Sn) = 139 Hz, 8H, CH₂), 5.44 ppm (s, 8H, NH₂); ¹³C NMR (75 MHz, CDCl₃): δ = 17.20 (Me), 27.90 (Me₂), 35.68 (CSn), 51.49 (CH₂), 151.75 ppm (CN); ¹¹⁹Sn NMR (187 MHz, CD₂Cl₂): δ = -680 ppm; ¹²⁵Te NMR (158 MHz, CD₂Cl₂): δ = 483, -660 ppm; IR: $\tilde{\nu}$ = 3339.2 (w), 3251.2 (w), 3143.5 (w), 3029.8 (w), 2952.1 (w), 2928.6 (w), 2882.4 (m), 2829.4 (m), 1499.8 (w), 1456.8 (w), 1407.4 (w), 1359.8 (m), 1258.7 (w), 1240.1 (w), 1194.6 (w), 1121.7 (m), 1093.3 (s), 967.7 (m), 799.4 (m), 698.6 (w), 653.6 (w), 505.5 cm⁻¹ (m); UV/Vis (onset): 1.8 eV; HRMS (ESI): *m/z* calcd for C₁₈H₃₉N₆Sn₃Te₄: 1206.6494 ([M-C₆H₁₃N₂SnTe₂]⁺); found: 1206.6494; EDX: calcd Sn/Te = 0.67:1.00; found: Sn/Te = 0.68:1.00.

Compound 6: Compound **2** (0.050 g, 0.066 mmol) was dissolved in dichloromethane (10 mL). Phenylhydrazine (0.022 g, 0.203 mmol) was added at room temperature. After 30 min, the solution was layered with *n*-hexane (10 mL). Red crystals of compound **6** formed within one day, which were collected and dried in high vacuum. Yield: 35 mg (0.021 mmol, 64% calculated on the basis of **2**). ¹H NMR (300 MHz, CD₂Cl₂): δ = 1.20 (s, ³J(¹H-¹¹⁹Sn) = 120 Hz), 18H, Me₂), 1.92 (s, 9H, Me), 2.39 (s, ³J(¹H-¹¹⁹Sn) = 129 Hz, 6H, CH₂), 3.53 (brs, 3H, NH), 6.70–7.20 ppm (m, 15H, Ph); ¹¹⁹Sn NMR (149 MHz, CD₂Cl₂): δ = 48 (SnCl), -626 ppm (SnTe); ¹²⁵Te NMR (158 MHz, CD₂Cl₂): δ = 449 (μ₃-Te), -844 ppm (μ₂-Te); IR: $\tilde{\nu}$ = 3650.6 (w), 3318.1 (w), 3206.3 (w), 2980.6 (m), 2883.1 (m), 2838.3 (m), 2707.4 (w), 2371.0 (w), 1598.6 (s), 1493.8 (s), 1453.1 (m), 1363.1 (m), 1333.1 (w), 1306.1 (w), 1250.0 (m), 1210.6 (s), 1170.1 (m), 1132.5 (s), 1067.9 (m), 994.5 (w), 962.1 (w), 885.2 (w), 800.9 (w), 744.3 (s), 690.4 (s), 655.7 (w), 584.1 (w), 504.1 (m), 450.6 cm⁻¹ (w); HRMS (ESI): *m/z* calcd for C₃₆H₅₁N₆Sn₃Te₄: 1434.7439 ([M-SnCl₃]⁺); found: 1434.7449; EDX: calcd Sn/Te = 1.00:1.00, found Sn/Te = 0.97:1.00.

Compound 7: A saturated solution of **6** in CD₂Cl₂ was sealed in an NMR test tube. After two weeks at room temperature, red crystals of compound **7**·3CH₂Cl₂ grew inside the tube, which were collected and dried in high vacuum. An alternative route for the directed synthesis of **7** is as follows: Compound **4** (0.020 g, 0.012 mmol) was dissolved in dichloromethane (5 mL). Phenylhydrazine (0.01 g, 0.09 mmol) was added at room temperature. The solution was stirred for one hour and subsequently layered with *n*-hexane (10 mL). Yield: 0.007 g (0.003 mmol, 25% calculated on the basis of **6**). ¹H NMR (300 MHz, CD₂Cl₂): δ = 1.16 (s, 24H, Me₂), 2.06 (s, 12H,

Me), 2.45 (s, 9H, CH₂), 3.60 (brs, 4H, NH), 6.80–7.30 ppm (m, 20H, Ph); EDX: calcd Sn/Te = 0.67:1.00, found Sn/Te = 0.65:1.00.

Compound 8: Compound **2** (0.050 g, 0.066 mmol) and 4-phenylthiosemicarbazide (0.022 g, 0.203 mmol) were dissolved in dichloromethane (10 mL). After 1 h, the solution was layered with *n*-hexane (10 mL). Yellow crystals of compound **8** formed within one week, which were collected and dried in high vacuum. Yield: 18 mg (0.018 mmol, 27% calculated on the basis of **2**). ¹H NMR (500 MHz, CD₂Cl₂): δ = 1.13 (s, 6H, ³J(¹H-¹¹⁹Sn) = 150 Hz, Me₂), 1.20 (s, 6H, ³J(¹H-¹¹⁹Sn) = 147 Hz, Me₂), 2.17 (s, 3H, CH₂), 2.18 (s, 3H, CH₂), 2.32 (s, 3H, ³J(¹H-¹¹⁹Sn) = 152 Hz, Me), 2.37 (s, 3H, ³J(¹H-¹¹⁹Sn) = 153 Hz, CH₂), 6.74 (s, 1H, NH), 6.80 (s, 1H, NH), 7.02–7.06 (m, 2H, Ph), 7.28–7.33 (m, 4H, Ph), 7.56–7.61 ppm (m, 4H, Ph); ¹³C NMR (125 MHz, CD₂Cl₂): δ = 24.72 (Me₂), 24.90 (Me₂), 29.98 (Me), 30.10 (Me), 37.26 (CSn), 37.60 (CSn), 47.88 (CH₂), 47.95 (CH₂), 120.32 (Ph), 120.37 (Ph), 123.37 (Ph), 129.44 (Ph), 139.74 (Ph), 150.12 (CN), 150.53 ppm (CN); ¹¹⁹Sn NMR (187 MHz, CD₂Cl₂): δ = -601, -605 ppm; ¹²⁵Te NMR (158 MHz, CD₂Cl₂): no signal found; IR: $\tilde{\nu}$ = 3660.9 (w), 2840.1 (m), 2710.8 (w), 1690.7 (s), 1451.2 (w), 1359.8 (s), 1172.1 (s), 1130.3 (s), 1013.2 (s), 959.6 (m), 876.8 (w), 796.5 (s), 744.5 (m), 607.5 (m), 485.5 (w), 437.2 (w), 406.4 cm⁻¹ (w); HRMS (ESI): *m/z* calcd for C₂₆H₃₅N₆S₂Sn₂Te₂: 988.8502 ([M+H]⁺); found: 988.8511; EDX: calcd S/Sn/Te = 1.00 :1.00:1.00, found S/Sn/Te = 0.98:1.00:0.96. The doublet set of signals in the NMR spectra is presumably caused by a *trans/cis* equilibrium in solution. For further details, see the DFT part below.

Compound 9: Compound **4** (0.050 g, 0.031 mmol) was dissolved in dichloromethane (5 mL). 4-phenylthiosemicarbazide (0.021 g, 0.124 mmol), dissolved in methanol (5 mL), was added at room temperature. After 1 h, the solution was layered with *n*-hexane (10 mL). Red crystals of **9**·2MeOH formed within one week, which were collected and dried in high vacuum. Yield: A few single crystals, which were insoluble in organic solvents. EDX: calcd S/Sn/Te = 0.33:0.67:1.00; found: S/Sn/Te = 0.35:0.68:1.00.

Isolation of compounds 10–12: Compound **2** (0.100 g, 0.131 mmol) was dissolved in dichloromethane (10 mL). Carbohydrazide (0.014 g, 0.155 mmol) was added at room temperature. The solution was stirred for 30 min and subsequently layered with *n*-hexane (10 mL). Colorless crystals of **10**·CH₂Cl₂, yellow crystals of **11**·1.5CH₂Cl₂, and red crystals of **12**·5CH₂Cl₂ formed within one week side by side. Single crystals of **12**·5CH₂Cl₂ were transformed under retention of the macroscopic morphology of the crystals into **12**·2CH₂Cl₂ in inert oil within 24 h. The determination of the individual yields was not possible due to the mixture of compounds. EDX of **10**: calcd Sn/Te = 1.00:0.50; found: Sn/Te = 1.00:0.53 (chlorine was not considered because of the dichloromethane solvent molecules). EDX of **11**: calcd Sn/Te = 1.00:0.33; found Sn/Te = 1.00:0.35 (chlorine was not considered because of the dichloromethane solvent molecules). EDX of **12**: calcd Sn/Te = 1.00:0.88, found Sn/Te = 1.00:0.90 (chlorine was not considered because of the dichloromethane solvent molecules).

X-ray crystallography

Data collection was performed on STOE IPDS2 and IPDS2t diffractometers using graphite-monochromatized Mo_{Kα} radiation (λ = 0.71073 Å) at 100 K (**4**·4CH₂Cl₂ was measured at 250 K). Structure solution and refinement by direct methods and full matrix least-squares on *F*², respectively; SHELXTL software.^[33] Details of the measurements, structure solutions and refinements as well as additional are provided in the Supporting Information. CCDC 1059622 ((Me₂Si)₂Te), 1059623 (**1**), 1059624 (**2**), 1059625 (**3**), 1059626 (**4**·4CH₂Cl₂), 1059627 (**5**), 1059628 (**6**·C₆H₁₄), 1059629 (**7**·3CH₂Cl₂),

1059630 (8), 1059631 (9·2MeOH), 1059632 (10·CH₂Cl₂), 1059633 (11·1.5CH₂Cl₂), 1059634 (12·5CH₂Cl₂), and 1059635 (12·2CH₂Cl₂) contain the supplementary crystallographic data for this paper. These data are provided free of charge by The Cambridge Crystallographic Data Centre.

Acknowledgements

Financial support by the Deutsche Forschungsgemeinschaft within the framework of GRK1782 is gratefully acknowledged.

Keywords: cluster compounds · density functional calculations · tellurium · tin · X-ray diffraction

- [1] a) A. L. Seligson, J. Arnold, *J. Am. Chem. Soc.* **1993**, *115*, 8214–8220; b) H. Borrmann, J. Campbell, D. A. Dixon, H. P. A. Mercier, A. M. Pirani, G. J. Schrobilgen, *Inorg. Chem.* **1998**, *37*, 6656–6674; c) A. Pop, L. Wang, V. Dorcet, T. Roisnel, J. F. Carpentier, A. Silvestru, Y. Sarazin, *Dalton Trans.* **2014**, *43*, 16459–16474; d) G. Thiele, T. Krüger, S. Dehnen, *Angew. Chem. Int. Ed.* **2014**, *53*, 4699–4703; *Angew. Chem.* **2014**, *126*, 4787–4891.
- [2] a) C. L. Bowes, G. A. Ozin, *Adv. Mater.* **1996**, *8*, 13–28; b) S. Bag, P. N. Trikalitis, P. J. Chupas, G. S. Armatas, M. G. Kanatzidis, *Science* **2007**, *317*, 490–493; c) M. V. Kovalenko, W. Heiss, E. V. Shevchenko, J.-S. Lee, H. Schwinghammer, A. P. Alivisatos, D. V. Talapin, *J. Am. Chem. Soc.* **2007**, *129*, 11354–11355; d) M. V. Kovalenko, M. Scheele, D. V. Talapin, *Science* **2009**, *324*, 1417–1420; e) Y. Tanaka, Z. Ren, T. Sato, K. Nakayama, S. Souma, T. Takahashi, K. Segawa, Y. Ando, *Nat. Phys.* **2012**, *8*, 800–803; f) T. Řičica, L. Strižik, L. Dostál, M. Bouška, M. Vlček, L. Beneš, T. Wágner, R. Jambor, *Appl. Organomet. Chem.* **2015**, *29*, 176–180.
- [3] M. G. Kanatzidis, *Adv. Mater.* **2007**, *19*, 1165–1181.
- [4] a) B. Eisenmann, H. Schäfer, H. Schrod, *Z. Naturforsch. Teil B* **1983**, *38*, 921–923; b) C. R. Evenson IV, P. K. Dorhout, *Z. Kristallogr. New Cryst. Struct.* **2000**, *215*, 318; c) A. M. Pirani, H. P. A. Mercier, D. A. Dixon, H. Borrmann, G. J. Schrobilgen, *Inorg. Chem.* **2001**, *40*, 4823–4829; d) K. Tsamourtzis, J.-H. Song, T. Bakas, A. J. Freeman, P. N. Trikalitis, M. G. Kanatzidis, *Inorg. Chem.* **2008**, *47*, 11920–11929.
- [5] a) G. Thiele, S. Peter, M. Schwarzer, E. Ruzin, R. Clérac, H. Staesche, C. Rosser, B. Roling, S. Dehnen, *Inorg. Chem.* **2012**, *51*, 3349–3351; b) E. Ruzin, A. Fuchs, S. Dehnen, *Chem. Commun.* **2006**, 4796–4798.
- [6] a) A. Schäfer, M. Weidenbruch, W. Saak, S. Pohl, H. Marsmann, *Angew. Chem. Int. Ed. Engl.* **1991**, *30*, 834–836; *Angew. Chem.* **1991**, *103*, 873–874; b) I. S. Chuprakov, K.-H. Dahmen, J. J. Schneider, J. Hagen, *Chem. Mater.* **1998**, *10*, 3467–3470; c) U. Herzog, G. Rheinwald, *J. Organomet. Chem.* **2001**, *627*, 23–36; d) M. Saito, H. Hashimoto, T. Tajima, *Acta Crystallogr. E* **2010**, *66*, m885–m886; e) J. Beckmann, D. Heinrich, S. Mebs, *Z. Anorg. Allg. Chem.* **2013**, *639*, 2129–2133.
- [7] a) K. Merzweiler, H. Kraus, *Z. Naturforsch. B* **1994**, *49*, 621–626; b) C. Wagner, R. Hauser, K. Merzweiler, *Phosphorus Sulfur Silicon Relat. Elem.* **2001**, *168*, 191–197; c) H. Braunschweig, R. Dörfler, K. Köhler, K. Radacki, *Organometallics* **2011**, *30*, 305–312; d) S. Traut, C. von Hänisch, A. P. Hähnel, S. Stahl, *Chem. Commun.* **2012**, *48*, 6984–6986; e) Z. You, J. Bergunde, B. Gerke, R. Pöttgen, S. Dehnen, *Inorg. Chem.* **2014**, *53*, 12512–12518.
- [8] a) W.-P. Leung, W.-H. Kwok, L. T. C. Law, Z.-Y. Zhou, T. C. W. Mak, *Chem. Commun.* **1996**, 505–506; b) W.-P. Leung, W.-H. Kwok, Z.-Y. Zhou, T. C. W. Mak, *Organometallics* **2000**, *19*, 296–303.
- [9] a) B. Mairychová, L. Dostál, A. Růžicka, M. Fulem, K. Růžicka, A. Lyčka, R. Jambor, *Organometallics* **2011**, *30*, 5904–5910; b) M. Bouška, L. Dostál, Z. Padělková, A. Lyčka, S. Herres-Pawlis, K. Jurkschat, R. Jambor, *Angew. Chem. Int. Ed.* **2012**, *51*, 3478–3482; *Angew. Chem.* **2012**, *124*, 3535–3540; c) M. Bouška, L. Strižik, L. Dostál, A. Růžicka, A. Lyčka, L. Beneš, M. Vlček, J. Příkryl, P. Knotek, T. Wágner, R. Jambor, *Chem. Eur. J.* **2013**, *19*, 1877–1881.
- [10] a) Z. Hassanzadeh Fard, L. Xiong, C. Müller, M. Hołyńska, S. Dehnen, *Chem. Eur. J.* **2009**, *15*, 6595–6604; b) S. Heimann, M. Hołyńska, S. Dehnen, *Z. Anorg. Allg. Chem.* **2012**, *638*, 1663–1666; c) J. P. Eußner, S. Dehnen, *Chem. Commun.* **2014**, *50*, 11385–11388; d) J. P. Eußner, B. E. Barth, U. Justus, N. W. Rosemann, S. Chatterjee, S. Dehnen, *Inorg. Chem.* **2015**, *54*, 22–24.
- [11] J. P. Eußner, B. E. K. Barth, E. Leusmann, Z. You, N. Rinn, S. Dehnen, *Chem. Eur. J.* **2013**, *19*, 13792–13802.
- [12] a) TURBOMOLE Version 6.2, TURBOMOLE GmbH 2011. TURBOMOLE is a development of University of Karlsruhe and Forschungszentrum Karlsruhe, **1989–2007**; Ridft program: b) K. Eichkorn, O. Treutler, H. Öhm, M. Häser, R. Ahlrichs, *Chem. Phys. Lett.* **1995**, *242*, 652–660; c) K. Eichkorn, F. Weigend, O. Treutler, R. Ahlrichs, *Theor. Chem. Acc.* **1997**, *97*, 119–124; B3LYP functional: d) C. Lee, W. Yang, R. G. Parr, *Phys. Rev.* **1988**, *37*, 785–789; TZVP basis sets: e) F. Weigend, R. Ahlrichs, *Phys. Chem. Chem. Phys.* **2005**, *7*, 3297–3305; f) F. Weigend, *Phys. Chem. Chem. Phys.* **2006**, *8*, 1057–1065; ECPs: g) B. Metz, H. Stoll, M. Dolg, *J. Chem. Phys.* **2000**, *113*, 2563–2569; electronic excitations: h) R. Bauernschmitt, R. Ahlrichs, *Chem. Phys. Lett.* **1996**, *256*, 454–464; i) R. Bauernschmitt, M. Häser, O. Treutler, R. Ahlrichs, *Chem. Phys. Lett.* **1997**, *264*, 573–578; j) S. Grimme, F. Furche, R. Ahlrichs, *Chem. Phys. Lett.* **2002**, *361*, 321–328; k) F. Furche, D. Rappoport, *Computational and Theoretical Chemistry, Vol. 16* (Ed.: M. Olivucci), Elsevier, Amsterdam, **2005**, pp. 93–138; Escf program: l) R. Bauernschmitt, R. Ahlrichs, *J. Chem. Phys.* **1996**, *104*, 9047–9052. Further details of the DFT calculations are provided in the Supporting Information.
- [13] HRMS (ESI) calcd for [C₁₈H₃₃O₃Sn₃Te₄]⁺: *m/z* = 1164.5688; found: 1164.5713.
- [14] The reductive elimination of organic ligands was also discussed for the generation of [(R¹-²Sn)₃Se₄][SnCl₃] (see ref. [11]).
- [15] Z. Hassanzadeh Fard, M. Hołyńska, S. Dehnen, *Inorg. Chem.* **2010**, *49*, 5748–5752.
- [16] S. Heimann, M. Hołyńska, S. Dehnen, *Chem. Commun.* **2011**, *47*, 1881–1883.
- [17] V. Pore, T. Hatanpää, M. Ritala, M. Leskelä, *J. Am. Chem. Soc.* **2009**, *131*, 3478–3480.
- [18] P. Pyykkö, M. Atsumi, *Chem. Eur. J.* **2009**, *15*, 186–197.
- [19] F. W. B. Einstein, I. D. Gay, C. H. W. Jones, R. D. Sharma, *Acta Crystallogr. C* **1993**, *49*, 470–472.
- [20] a) K. Jurkschat, S. van Dreumel, G. Dyson, D. Dakternieks, T. J. Bastow, M. E. Smith, M. Dräger, *Polyhedron* **1992**, *11*, 2747–2755; b) D. Dakternieks, K. Jurkschat, H. Wu, E. R. T. Tiekink, *Organometallics* **1993**, *12*, 2788–2793.
- [21] A. Bondi, *J. Phys. Chem.* **1964**, *68*, 441–451.
- [22] J. Beckmann, J. Bolsinger, A. Duthie, *Chem. Eur. J.* **2011**, *17*, 930–940.
- [23] The N atoms still occupy the “trans” positions of a pseudo trigonal bipyramidal coordination arrangement (N1–Sn1–Te1: 168.7(1)°, N3–Sn2–Te1: 173.1(1)°). Though C–Sn distances of the *ipso* C atoms of C1 and C13 are shorter than 3.1 Å, resulting in coordination polyhedra with a higher number of vertices.
- [24] J. P. Eußner, S. Dehnen, *Z. Anorg. Allg. Chem.* **2012**, *638*, 1827–1832.
- [25] A. W. Addison, T. N. Rao, J. Reedijk, J. van Rijn, G. C. Verschoor, *J. Chem. Soc. Dalton Trans.* **1984**, 1349–1356.
- [26] J. Beckmann, D. Dakternieks, A. Duthie, C. Jones, K. Jurkschat, E. R. T. Tiekink, *J. Organomet. Chem.* **2001**, *636*, 138–143.
- [27] C. H. W. Jones, R. D. Sharma, S. P. Taneja, *Can. J. Chem.* **1986**, *64*, 980–986.
- [28] The bond energies were calculated according to Equations (3) and (4) in the Supporting Information.
- [29] A. E. Reed, R. B. Weinstock, F. Weinhold, *J. Phys. Chem.* **1985**, *83*, 735–746.
- [30] *E*_{onset} (1) = 2.6 eV, *E*_{onset} (2) = 2.1 eV, *E*_{onset} (3) = 1.9 eV.
- [31] R. E. Hutton, J. W. Burley, *J. Organomet. Chem.* **1978**, *156*, 369–382.
- [32] a) M. Schmidt, H. Ruf, *Angew. Chem.* **1961**, *73*, 64; b) M. Schmidt, H. Ruf, *Z. Anorg. Allg. Chem.* **1963**, *321*, 270–273.
- [33] G. M. Sheldrick, *Acta Crystallogr. A* **2008**, *64*, 112–122.

Received: April 28, 2015

Published online on July 23, 2015